

PACIFIC EARTHQUAKE ENGINEERING RESEARCH CENTER

Ground Failure of Hydraulic Fills in Chiba, Japan and Data Archival in Community Database

**Scott J. Brandenberg
Jonathan P. Stewart
Kenneth S. Hudson
Dong Youp Kwak
Paolo Zimmaro
Quin Parker**

**Department of Civil and Environmental Engineering
University of California, Los Angeles, California**

Ground Failure of Hydraulic Fills in Chiba, Japan and Data Archival in Community Database

Scott J. Brandenberg

Jonathan P. Stewart

Kenneth S. Hudson

Dong Youp Kwak

Paolo Zimmaro

Quin Parker

Department of Civil and Environmental Engineering
University of California, Los Angeles, California

PEER Report 2024/06
Pacific Earthquake Engineering Research Center
Headquarters at the University of California, Berkeley
July 2024

ABSTRACT

This report describes analysis of ground failure and lack thereof observed in the Mihama Ward portion of Chiba, Japan following the 2011 M9.0 Tohoku Earthquake. In conjunction with this work, we have also significantly expanded the laboratory component of the Next Generation Liquefaction (NGL) relational database.

The district referred to as Mihama Ward is on ground composed of hydraulic fill sluiced in by pipes, thereby resulting in a gradient of soil coarseness, with coarser soils deposited near the pipes and fine-grained soils carried further away. Observations from local researchers at Chiba University following the 2011 Tohoku Earthquake indicate that ground failure was observed closer to the locations where the pipes deposited the soil, and not further away. This ground failure consisted of extensive sand boiling and ground cracking, which led to building settlement and pipe breaks. Our hypothesis at the outset of the project was that liquefaction susceptibility might explain the pattern of ground failure. Specifically, soils deposited near the pipes are susceptible due to their coarser texture, while soils further from the pipes may be non-susceptible due to the presence of clay minerals and higher plasticity. Were this hypothesis borne out by evidence, soil in the transition zone would have provided important insights about liquefaction susceptibility. Based on testing of soils in our laboratory, we find this hypothesis to be only partially correct. We have confirmed that there are regions with high clay contents and no ground failure and other regions with predominantly granular soils and extensive surface manifestation of liquefaction. Where the hypothesis breaks down is in the transition zone, where we found that the fine-grained soils are non-plastic, and therefore they are susceptible to liquefaction. Our interpretation is that these silt materials likely liquefied during the earthquake, but did not manifest liquefaction. Two factors may have contributed to this lack of manifestation: (1) level ground conditions and lack of large driving static shear stresses (structures in the region are light residential construction) and (2) the silt is less likely to erode to the surface and form silt boils than the sandier soils that produced surface manifestations. This case history points to the importance of separating triggering (defined as the development of significant excess pore pressure and loss of strength) from manifestation (defined as observations of ground failure, including cracking, sand boils, and lateral spreading).

The Mihama Ward case history involved laboratory tests performed by Tokyo Soil Research Co. Ltd. and the UCLA geotechnical laboratory. Given the importance of this data to the understanding of this case history, we recognized a need to incorporate laboratory tests in the NGL database alongside field tests and liquefaction observations. We therefore developed an organizational structure for laboratory tests, including direct simple shear, triaxial compression, and consolidation, and implemented the schema in the NGL database. We then uploaded data from tests performed by Tokyo Soil and UCLA. Furthermore, numerous other researchers have also uploaded laboratory test data for other sites. This report describes the organizational structure of the laboratory component of the database, and a tool for interacting with laboratory data.

Keywords: Liquefaction, Tohoku Earthquake, Database, Laboratory, Triggering, Susceptibility

ACKNOWLEDGMENTS AND DISCLAIMER

This research study was funded by the California State Highway Fund through the Pacific Earthquake Engineering Research Center, under Contract No. 1153-NCTRIT. The opinions, findings, conclusions, and recommendations expressed in this publication are those of the author(s) and do not necessarily reflect the view of the State of California, Pacific Earthquake Engineering Research (PEER) Center, and the Regents of the University of California. The Next Generation Liquefaction Database, which was utilized extensively as part of this report, was financially supported by the U.S. Nuclear Regulatory Commission (NRC) and the U.S. Bureau of Reclamation (USBR) through the Southwest Research Institute (SWRI). Neither the U.S. Government nor any agency thereof, nor any of their employees, makes any warranty, expressed or implied, or assumes any legal liability or responsibility for any third party's use, or the results of such use, of any information, apparatus, product, or process disclosed in this paper, or represents that its use by such third party would not infringe privately owned rights. The views expressed in this report are not necessarily those of the NRC or USBR.

CONTENTS

ABSTRACT.....	III
ACKNOWLEDGMENTS AND DISCLAIMER	V
CONTENTS.....	VII
LIST OF TABLES	IX
LIST OF FIGURES	XI
1 INTRODUCTION.....	1
1.1 Definition of Terms	2
1.2 Motivation.....	5
2 MIHAMA WARD CASE HISTORY	8
2.1 Site Geologic History and Observed Field Performance.....	8
2.2 Cone Penetration Tests.....	11
2.3 Boring Logs.....	17
2.4 Triaxial Tests.....	22
2.5 Liquefaction Triggering Evaluation.....	22
3 LABORATORY SCHEMA FOR NGL DATABASE	30
3.1 Laboratory Database Schema.....	30
3.2 Database Population	33
3.2.1 Laboratories	33
3.2.2 Laboratory Test Programs.....	33
3.3 Accessing Through Graphical User Interface	36
3.4 Interacting with Data in DesignSafe	37
4 SUMMARY AND CONCLUSIONS	44
REFERENCES.....	46
APPENDIX A: TRIAXIAL TEST DATA	48

LIST OF TABLES

Table 1-1	Definition of terms in this report.	2
Table 2-1	Critical layer properties for CPT triggering evaluation.....	29
Table 3-1	Laboratories in NGL database (last accessed 07/15/2023).	33
Table 3-2	Laboratory test programs and number of tests in each program in NGL database. ..	35

LIST OF FIGURES

Figure 1.1	The head of the Fourth Avenue landslide induced by the 1964 Great Alaska Earthquake (Hansen 1965).....	2
Figure 1.2	Typical foundation failure (punched footings and intermediate slab heaving). (Chu et al. 2008). Photo by R. Seed (1999)	2
Figure 1.3	Comparison of “sand-like” behavior in cyclic triaxial testing of Sacramento River sand, and “clay-like” behavior exhibited by Cloverdale clay (Boulanger and Idriss 2007)	3
Figure 1.4	Cyclic triaxial test of clay specimen C11-P2A with PI=11 and LL=32 (Sancio 2003).	4
Figure 2.1	Reclamation process for Mihama ward during the 1970’s showing (a) discharge pipes used to place dredged soil, and (b) an aerial view of the discharge pipe locations (Nakai and Sekiguchi 2013).	8
Figure 2.2	Contour maps of (a) peak acceleration (Nakai and Sekiguchi 2013) and (b) observed sand boils (Sekiguchi and Nakai 2012).	9
Figure 2.3	Locations of study site 8 Chome Meeting Place. Surface manifestation locations from (Sekiguchi and Nakai 2012).	10
Figure 2.4	Cone penetration test CPT01.	11
Figure 2.5	Cone penetration test CPT02.	12
Figure 2.6	Cone penetration test CPT03.	12
Figure 2.7	Cone penetration test CPT04.	13
Figure 2.8	Cone penetration test CPT05.	13
Figure 2.9	Cone penetration test CPT06.	14
Figure 2.10	Cone penetration test CPT07.	14
Figure 2.11	Cone penetration test CPT08.	15
Figure 2.12	Cone penetration test CPT09.	15
Figure 2.13	Cross-section interpreted from CPT test data along transect A-A' from Fig. 2.3.	16
Figure 2.14	Cross-section interpreted from CPT test data along transect B-B from Fig. 2.3.	17
Figure 2.15	Boring log hatch legend.	17
Figure 2.16	Boring log for B1.	19

Figure 2.17	Boring log for B3.....	20
Figure 2.18	Boring log for B6.....	21
Figure 2.19	Liquefaction triggering evaluation of CPT001 (manifestation = yes).....	24
Figure 2.20	Liquefaction triggering evaluation of CPT002 (manifestation = yes).....	24
Figure 2.21	Liquefaction triggering evaluation of CPT003 (manifestation = no).....	25
Figure 2.22	Liquefaction triggering evaluation of CPT004 (manifestation = no).....	25
Figure 2.23	Liquefaction triggering evaluation of CPT005 (manifestation = no).....	26
Figure 2.24	Liquefaction triggering evaluation of CPT006 (manifestation = no).....	26
Figure 2.25	Liquefaction triggering evaluation of CPT007 (manifestation = no).....	27
Figure 2.26	Liquefaction triggering evaluation of CPT008 (manifestation = no).....	27
Figure 2.27	Liquefaction triggering evaluation of CPT009 (manifestation = yes).....	28
Figure 2.28	Critical layer selections plotted along with Boulanger and Idriss (2016) triggering curves. Open circles are manifestation = no, closed circles are manifestation = yes.	29
Figure 3.1	Relational database schema for laboratory component of database.....	32
Figure 3.2	Next-generation liquefaction graphical user interface. https://nextgenerationliquefaction.org/ accessed 07/15/2023.....	36
Figure 3.3	Example query of the number of tests of the various types stored in the NGL database.....	38
Figure 3.4	NGL laboratory test viewer GUI for selecting Lab Program and Sample.....	39
Figure 3.5	Direct simple shear test viewer example.....	40
Figure 3.6	Consolidation test viewer example.....	41
Figure A.1	Triaxial test on B6, sample S-1 for stage 1.....	48
Figure A.2	Triaxial test on B6, sample S-1 for stage 2.....	48
Figure A.3	Triaxial test on B6, sample S-1 for stage 3.....	49
Figure A.4	Triaxial test on B1, sample S-2, for stage 1.....	49
Figure A.5	Triaxial test on B1, sample S-2, for stage 2.....	50
Figure A.6	Triaxial test on B1, sample S-2, for stage 3.....	50
Figure A.7	Triaxial test on B1, sample S-3, for stage 1.....	51
Figure A.8	Triaxial test on B1, sample S-3, for stage 2.....	51
Figure A.9	Triaxial test on B1, sample S-3, for stage 3.....	52

1 INTRODUCTION

Liquefaction of cohesionless sandy and silty soils is a critical ground failure mechanism, having produced ground deformations and instabilities during many past earthquakes, including for example, tilting of the Kawagishi Cho apartment buildings in Niigata in 1964, settlement and tilting of small residential structures in Japan during the 2011 Tohoku earthquake, and destruction of many residences in New Zealand during the Canterbury earthquake sequence in 2010 and 2011. Additional striking occurrences of ground failure have occurred in fine-grained soils generally considered not susceptible to liquefaction. For example, the **M**9.3 1964 Great Alaska Earthquake induced two especially notable landslides, the Fourth Avenue and L Street slides, which damaged structures in Anchorage (Figure 1.1) as a result of the cyclic failure of Bootlegger Cove clay underlying a thick gravel deposit (Brandenberg and Idriss 2022; Idriss 1985). The **M**7.6 1999 Chi-Chi, Taiwan Earthquake induced significant incidents of ground failure in Wufeng, Taiwan, where peak ground accelerations on firm ground were about 0.7 g. Typical damage consisted of footings punching into the soil and intermediate slabs heaving, as shown in Fig. 1.2 (Chu et al. 2008). Soils beneath these structures were low-plasticity clays with water contents near the liquid limit. Similar failures were observed beneath structures in Adapazari, Turkey following the Kocaeli earthquake (e.g., (Bray et al. 2004) in soils with high fines contents and variable (but generally small) levels of plasticity. One of the striking features of these foundation failures involving fine-grained soils is that ground failure often did not occur in the free-field, being localized instead beneath foundations.



Figure 1.1 The head of the Fourth Avenue landslide induced by the 1964 Great Alaska Earthquake (Hansen 1965).



Figure 1.2 Typical foundation failure (punched footings and intermediate slab heaving). (Chu et al. 2008). Photo by R. Seed (1999)

1.1 DEFINITION OF TERMS

Clear definitions of the terminology surrounding susceptibility, liquefaction triggering, manifestation, and cyclic softening is warranted. The definition of these terms in the context of this report are provided below.

Table 1.1 Definition of terms in this report.

Term	Definition
Susceptibility	A characteristic of the minerals from which the soil is composed that controls whether a soil can liquefy if exposed to adequate cyclic stress while in a saturated condition.
Triggering	The sudden loss of strength and stiffness exhibited by susceptible soils
Cyclic Softening	The gradual loss of strength and stiffness exhibited by non-susceptible soils
Manifestation	Disruptions of the ground surface, structural settlement, or any other observable outcomes of liquefaction or cyclic softening

Susceptibility

We define susceptibility as a characteristic of the minerals from which the soil is composed. This definition of susceptibility is consistent with that adopted in the NGL project, but is not universal within the geotechnical community (Stuedlein et al. 2023), and we discuss several alternatives later. According to our definition, soils that are susceptible to liquefaction are composed of “bulky” minerals with low specific surface area (i.e., the ratio of surface area to mass). The strength and stiffness of susceptible soil is derived from mechanical inter-particle contact forces controlled by gravity loading. These minerals may be coarse-grained sand and gravel particles, or fine-grained silt particles. Soils that are not susceptible to liquefaction are composed of clayey minerals with high specific surface area. Electro-chemical interactions between surfaces of clay minerals give rise to plasticity for non-susceptible soils, making them moldable and “sticky”.

Differences in the cyclic behavior of susceptible and non-susceptible soils are shown in Fig. 1.3 for Sacramento River sand (susceptible) and Cloverdale clay (non-susceptible). The Sacramento River sand exhibits stress-strain curves that have an inverted s-shape, and have very little shear resistance at zero strain after liquefaction. Furthermore, strain develops rapidly after liquefaction, in a manner that is well-described by the term “triggering.” By contrast, the Cloverdale clay exhibits fatter hysteresis loops, and more significant resistance at zero strain. Furthermore, the clay exhibits a gradual increase of strain with each loading cycle in a manner that is well described by the phrase “cyclic softening”. In both cases the soil accumulates inelastic strain with increased loading cycles, indicating degradation of the soil fabric and loss of cyclic strength. Therefore, both types of soil are capable of producing earthquake-induced ground failure.

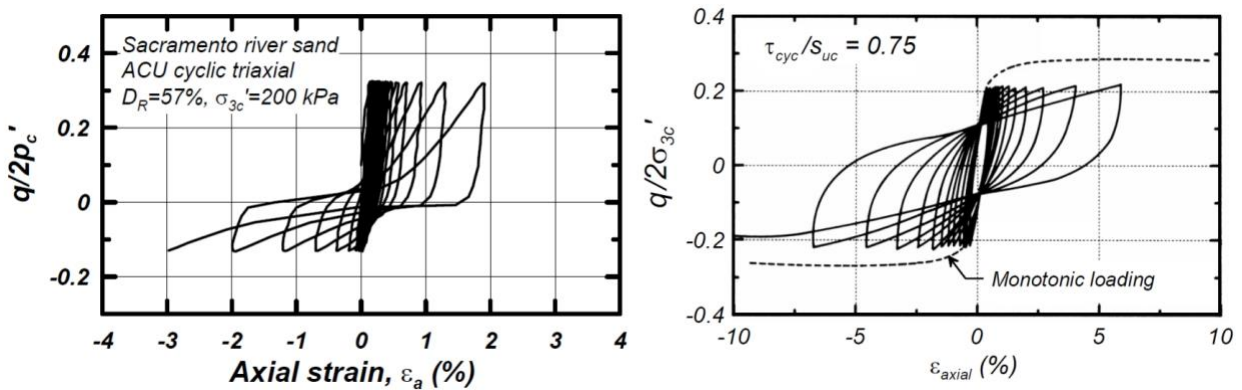


Figure 1.3 Comparison of “sand-like” behavior in cyclic triaxial testing of Sacramento River sand, and “clay-like” behavior exhibited by Cloverdale clay (After Boulanger and Idriss 2004)

Soils are often composed of a mixture of bulky and clayey minerals, resulting in transitional behavior intermediate between the limiting cases of sand- and clay-like soil behavior rather than a hard boundary. Fig. 1.4 illustrates a soil with stress-strain behavior that exhibits aspects of clay-like and sand-like behavior. The soil exhibits a slight inverted s-shaped behavior, and a gradual accumulation of strain. This soil has a plasticity index, $PI = 11$, and is likely composed of a combination of bulky and clayey minerals, both of which influence the mechanical response to cyclic loading.

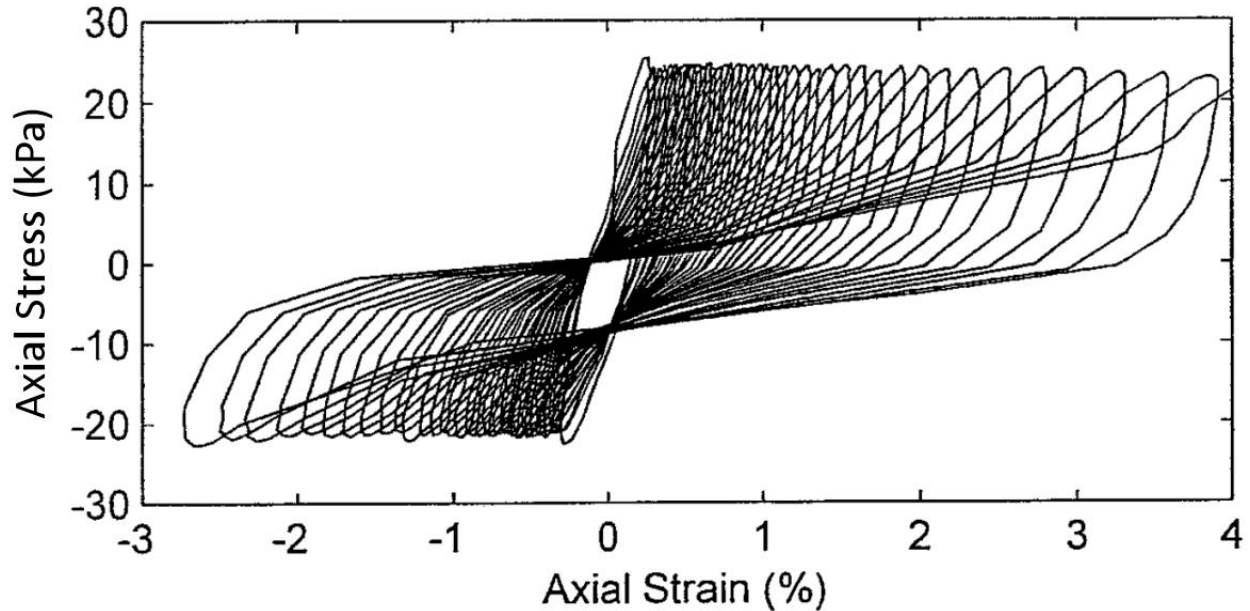


Figure 1.4 Cyclic triaxial test of clay specimen C11-P2A with PI=11 and LL=32 (Sancio 2003).

Other definitions of susceptibility include soil state (e.g., water content or density), degree of saturation, and drainage conditions. For example, Bray and Sancio (2006) define susceptibility in terms of plasticity index, which pertains to mineral composition, and the ratio of water content to liquid limit, which pertains to soil state. According to this definition, a susceptible soil may become non-susceptible by becoming denser (or vice-versa). Similar definitions have been proposed by other researchers [e.g., Wang (1979); Seed and Idriss (1982)]. Unsaturated soils are often defined as being non-susceptible due to the significant increase in liquefaction resistance that arises from the increased compressibility of the pore fluid, and matric suction associated with partial saturation. For example, a dry sand will not liquefy regardless of how strongly it is shaken. However, degree of saturation is transient. A dry soil may become saturated if groundwater rises, in which case it can liquefy during shaking. Furthermore, sandy soils with a degree of saturation less than unity have been observed to liquefy in laboratory studies [e.g., Tsukamoto et al. (2014)]. Gravel soils are sometimes considered non-susceptible to liquefaction based on the observation that they often drain quickly. However, gravel soils with drainage impeded by a capping layer have liquefied in past earthquakes.

A benefit of our definition of susceptibility is that it does not depend on changes in state or environmental factors such as groundwater table position or drainage conditions. It can therefore be considered a fundamental soil property. A potentially confusing aspect of our definition is that susceptible soils may sometimes have high cyclic strengths that will prevent liquefaction from occurring. It seems incongruous to say that a dry sand is susceptible to liquefaction because we acknowledge that dry sand will not liquefy. Our definition of susceptibility should therefore be viewed as guidance on the type of analysis to perform (triggering vs. cyclic softening) rather than as a statement of whether a particular layer is or is not problematic. Furthermore, adjustment factors should be applied to cyclic strength to account for factors such as saturation and drainage boundary conditions.

Triggering

Liquefaction triggering is the sudden loss of strength and stiffness of susceptible soils, and is most commonly caused by earthquake shaking but can also occur in response to sudden increases in shear stresses that are applied monotonically. Triggering is accompanied by high excess pore pressure ratios, and the soil often reaches a condition of zero effective stress. In stress-controlled cyclic laboratory testing, the point at which a soil triggers is often defined based on either reaching a threshold excess pore pressure ratio (e.g., 0.98 or 1.0), or when the soil reaches a threshold strain (e.g., 3% single amplitude).

Cyclic Softening

Cyclic softening is the gradual increase of shear strain exhibited by non-susceptible soils during cyclic loading. Excess pore pressures typically develop during cyclic softening, but the soil generally does not reach a condition of zero effective stress. Cyclic strength of non-susceptible soils is generally defined based on a strain-based threshold.

Manifestation

Manifestation is a disturbance of the ground surface arising from liquefaction or cyclic softening. Liquefaction triggering often manifests as sand boils that rise to the ground surface as a consequence of water eroding the soil particles through ground cracks and flowing to the surface due to upward hydraulic gradients induced by liquefaction. Lateral spreading often accompanies liquefaction triggering when a static shear stress is imposed on the ground due to surface slope, or a nearby free face. Liquefaction may trigger without causing surface manifestation. For example, a thick nonliquefiable crust might suppress manifestation of a deep liquefied layer. Furthermore, dense sands are less likely to manifest than loose sands because they are dilative and exhibit less strain in each cycle, and less volume change upon reconsolidation. Cyclic softening often manifests as ground cracks or lateral spreading at sites with slopes or a free-face, or as structural settlement or bearing capacity failure. In the latter case, manifestation is often observed in the vicinity of a structure, but not in the free-field. This indicates that soil-structure-interaction may play an important role in cyclic softening of non-susceptible soils.

1.2 MOTIVATION

This report consists of two components. First is analysis of a case history from the 2011 Tohoku earthquake at Mihama Ward. We pursued this case history initially because it presented promise for assessing liquefaction susceptibility because of a spatial variation of soil composition due to the manner in which the soil was deposited. Soils that exhibited surface evidence of liquefaction were found to be susceptible, while soils that did not exhibit surface evidence ranged from high plasticity clayey soils to nonplastic silts. Susceptibility was therefore a contributing factor, but other factors were also at play. We therefore focus most of our attention on triggering and manifestation of susceptible soils. The second component is an extension of the Next Generation Liquefaction (NGL) database to include laboratory test data. While there are disagreements in the

literature regarding the plasticity characteristics that cause a soil to be susceptible to liquefaction, there is near-universal agreement that laboratory testing of fine-grained soils is the best path forward for assessing strength loss potential. Laboratory test data is often presented through figures in papers and reports, and perhaps synthesized into summary plots, but the digital data files are often not made publicly available. Researchers often gain fundamental insights and make new discoveries by interpreting data in ways that differ from the interpretation methodologies adopted by the original author(s). We therefore present a relational database for laboratory tests, including the database schema, a description of the data in the database, and a tool for interacting with the laboratory data.

2 MIHAMA WARD CASE HISTORY

2.1 SITE GEOLOGIC HISTORY AND OBSERVED FIELD PERFORMANCE

Mihama Ward consists of reclaimed land in Chiba, Japan created by discharging soil dredged from the Tokyo Bay sea bed through pipes (Fig. 2.1). Placement of the dredged material commenced in the 1960's, and finished in the mid-1980's. The dredged material consists of a mix of sand, silt, and clay, which became mixed together during the pumping and transport process. Upon deposition through the discharge pipes, larger particles settle first, near the pipe location, while finer-grained particles were carried further away from the pipes. As a result, the soil texture and its susceptibility to liquefaction vary spatially in a manner that depends on distance from the discharge pipes. Fig. 2.1b shows aerial photographs from the time of reclamation in 1972 (Nakai and Sekiguchi 2013), including the locations of discharge pipes.

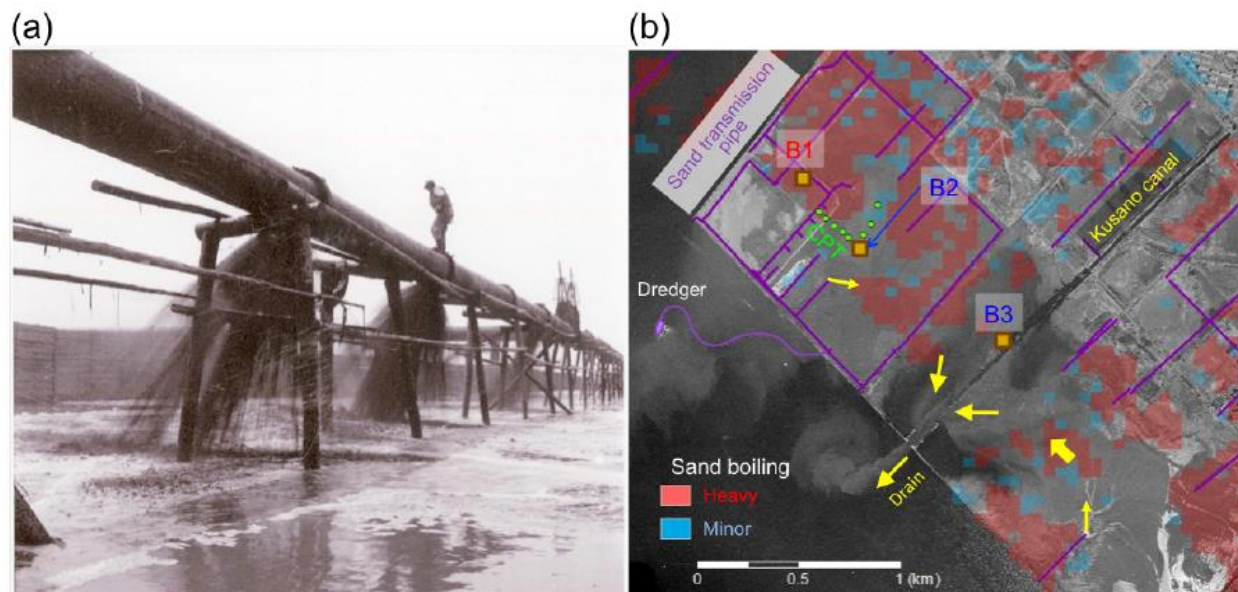


Figure 2.1 Reclamation process for Mihama ward during the 1970's showing (a) discharge pipes used to place dredged soil, and (b) an aerial view of the discharge pipe locations (Nakai and Sekiguchi 2013).

Following the M9 Tohoku-Oki earthquake on March 11, 2011, Chiba University dispatched a reconnaissance team to inspect Mihama ward (Sekiguchi and Nakai 2012). They visited accessible public areas, including roads and parks, and mapped locations with surface evidence of liquefaction in the form of sand boils. They classified sand boils as being heavy if the sand boil diameter was more than 1m, minor if the diameter was smaller than 1m, and none otherwise. The

team inspected most portions of Mihama ward, so zones without indications of sand boils can be confirmed as no evidence of no surface manifestation (as distinguished from a lack of evidence regarding manifestation).

Nakai and Sekiguchi (2013) developed a map of peak horizontal acceleration in Mihama ward, as shown in Fig. 2.2. They estimated shear wave velocity profiles based on soil layers from 540 borings in the region, and interpolated cells between borings. They then convolved a recording from the nearby Masago station to obtain a bedrock motion, and propagated the rock motion through the site using 1-D ground response analysis. Differences in PGA therefore represent differences in site conditions alone, without consideration for differences in path effects and source effects. However, these effects are anticipated to be essentially identical throughout Mihama ward based on the large rupture distance. The range of PGA values is 0.2 to 0.35g, which is strong enough to trigger liquefaction in many susceptible soils. Most SPT blow counts in Mihama ward are less than 10, with the exception of the unsaturated desiccated crust layer above the groundwater table (about 3m depth).

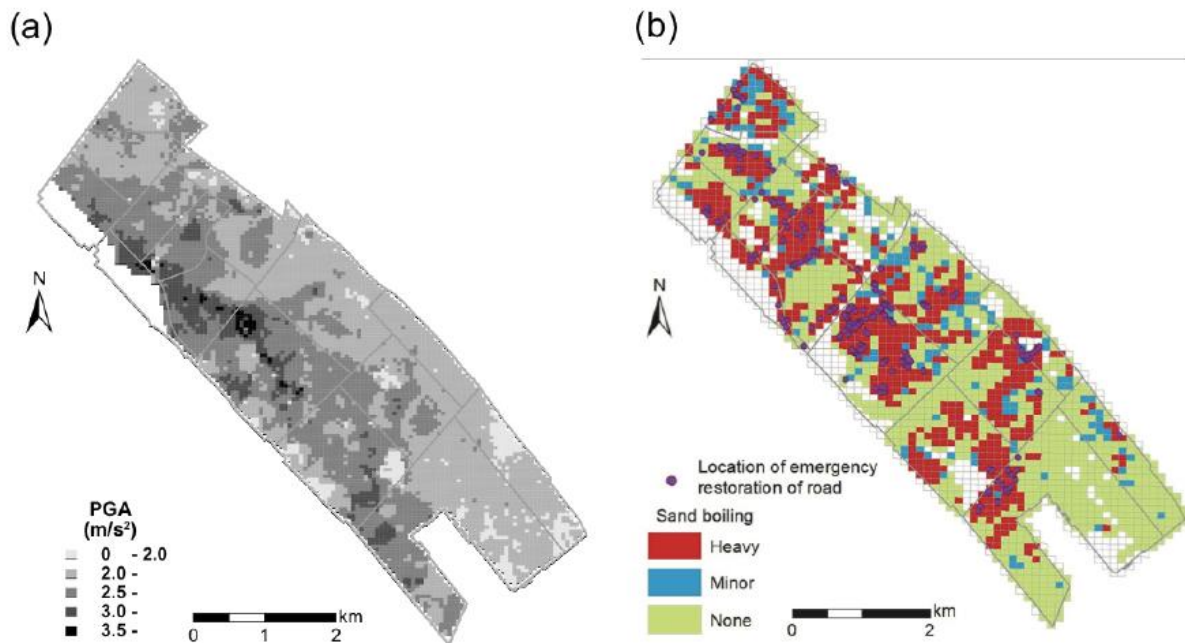


Figure 2.2 Contour maps of (a) peak acceleration (Nakai and Sekiguchi 2013) and (b) observed sand boils (Sekiguchi and Nakai 2012).

This study focuses on a location within Mihama ward, herein identified as 8 Chome Meeting Place, where cone penetration tests, boreholes, laboratory tests, and shear wave velocity measurements are available. Furthermore, the site was selected because it spans a range of observations of liquefaction from heavy to none, with heavy liquefaction occurring near the location where the

discharge pipe was located during reclamation, and no surface evidence observed further away from the discharge pipe, as shown in Fig. 2.3. Data presented in this study are available in the NGL database under site name “Mihama-Ward (8 Chome Meeting Place)”.

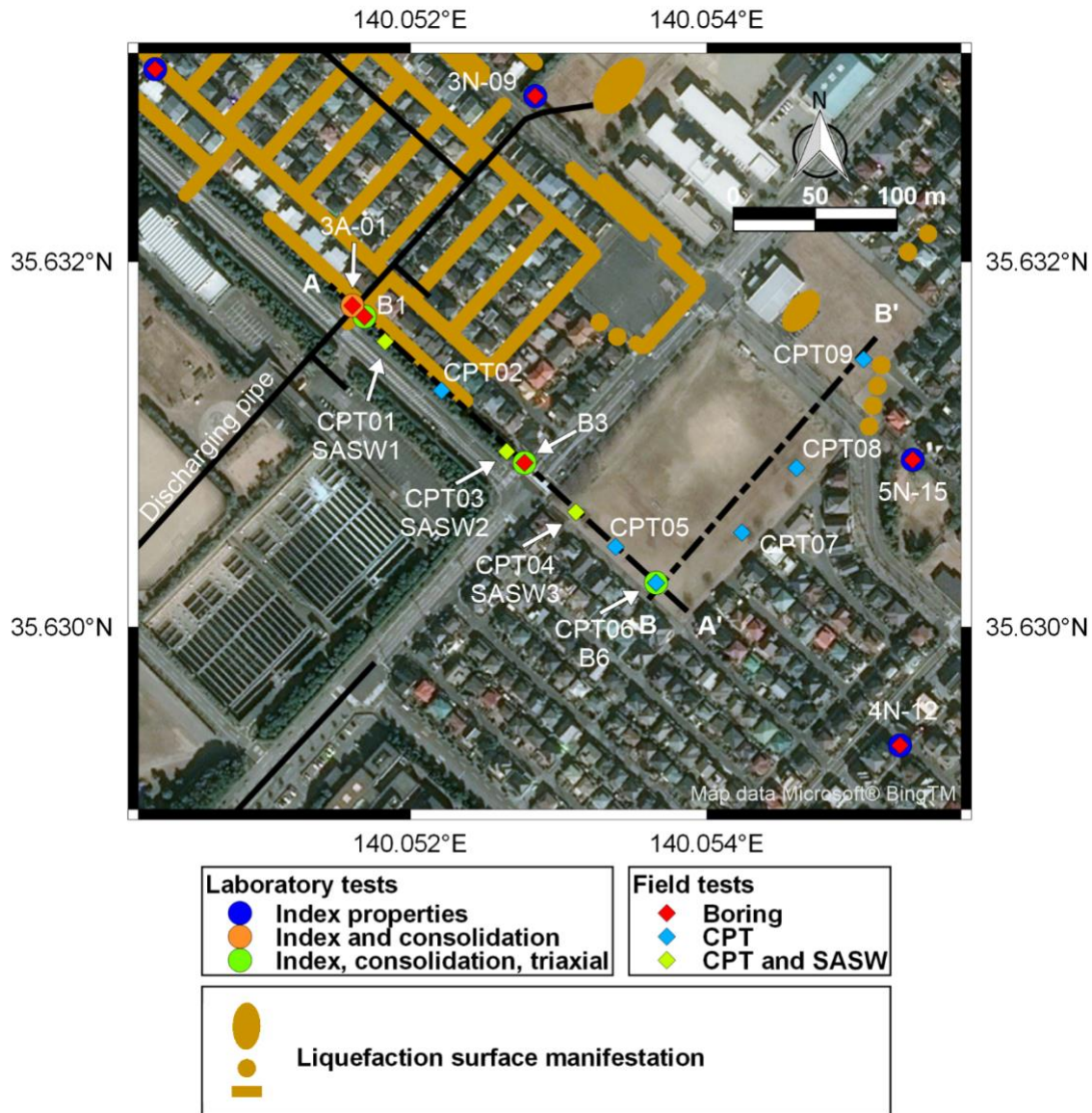


Figure 2.3 Locations of study site 8 Chome Meeting Place. Surface manifestation locations from (Sekiguchi and Nakai 2012).

Following observations of damage patterns, we formed a hypothesis that liquefaction susceptibility was responsible for the gradual transition from sand boiling near the discharge pipe to no surface evidence further away. Due to the spatial variation in soil composition, the 8 Chome Meeting Place location was identified as being extremely valuable for studying susceptibility. To evaluate soil

conditions, geotechnical site investigations were performed at locations shown in Fig. 2.3 by Chiba University and UCLA. Investigations include 9 cone penetration tests (CPTs) by Chiba, one boring with standard penetration test measurements by UCLA, and tube sampling of specific layers (B1, B3, and B6 in Fig. 2.3), followed by index, consolidation, and undrained strength testing by Tokyo Soil, Inc. Soils tested by Tokyo Soil were shipped to UCLA for additional index testing as well as consolidation and direct simple shear testing of reconstituted specimens.

2.2 CONE PENETRATION TESTS

The cone penetration test data are presented in Figs. 2.4 through 2.12. These plots include the measured cone tip resistance, q_t , and sleeve friction, f_s , along with the computed soil behavior type index, I_c , and associated soil behavior type, SBT_n . As anticipated, CPTs located closer to the discharge pipes (CPT 01 and 02) contain sandier soils, while finer grained soils are encountered further from the discharge pipes.

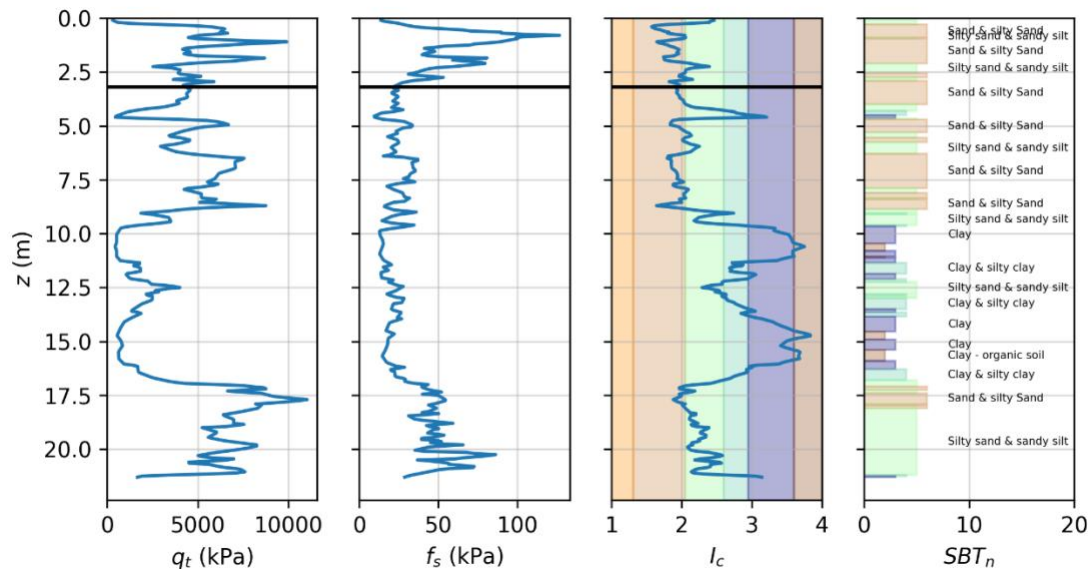


Figure 2.4 Cone penetration test CPT01.

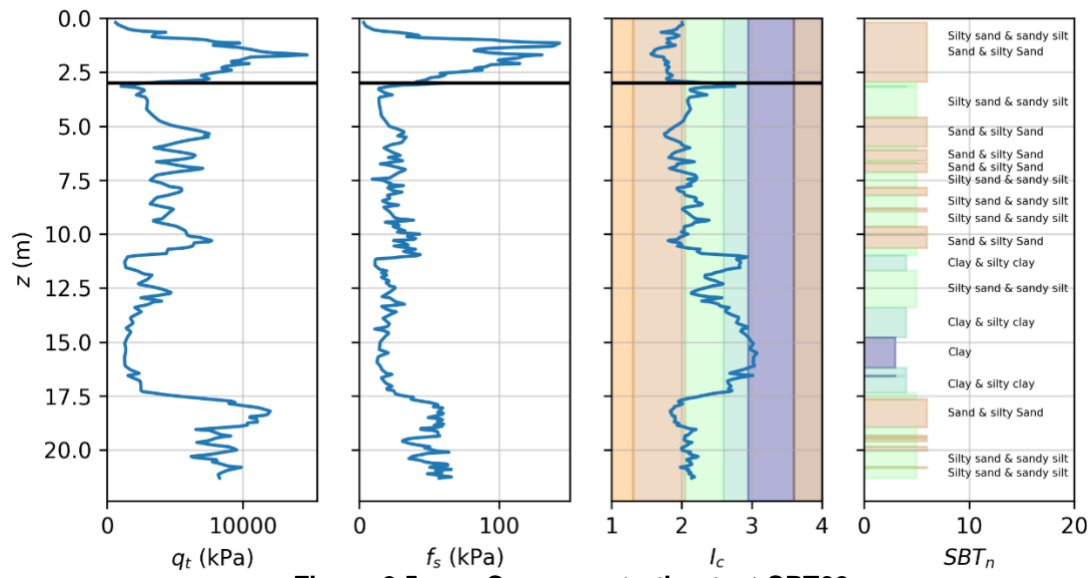


Figure 2.5 Cone penetration test CPT02.

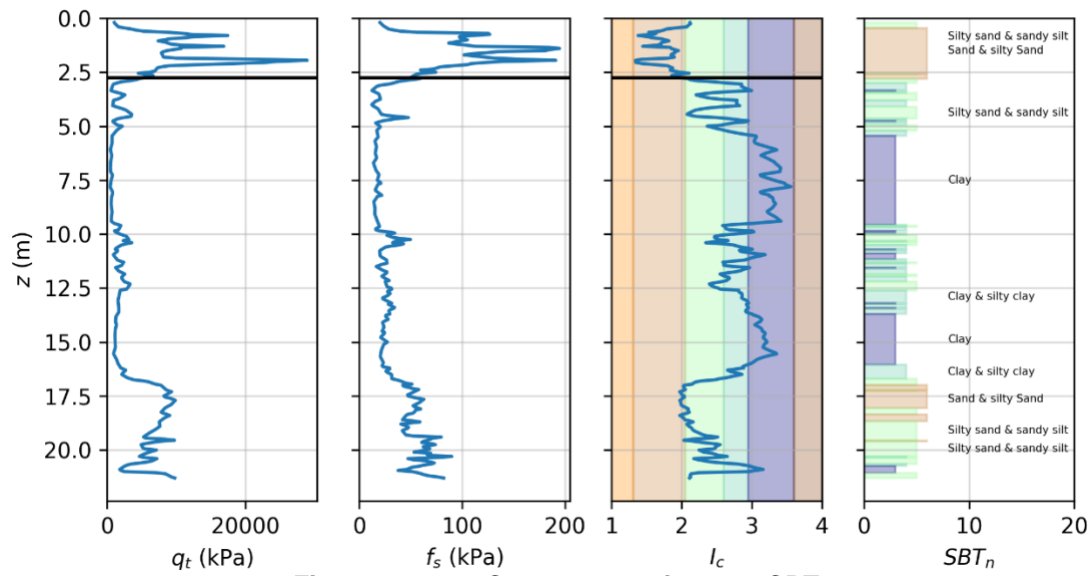


Figure 2.6 Cone penetration test CPT03.

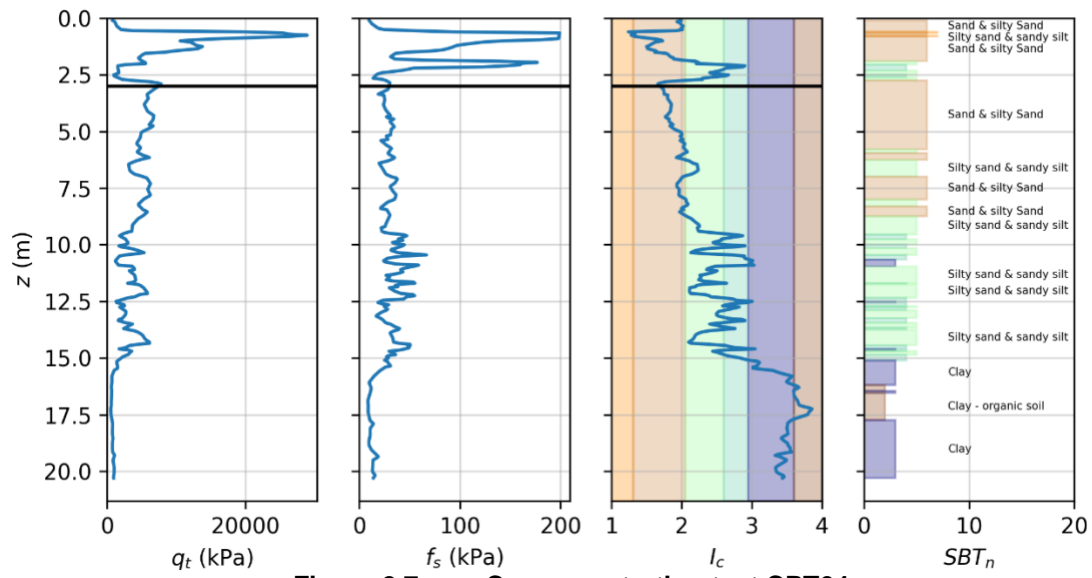


Figure 2.7 Cone penetration test CPT04.

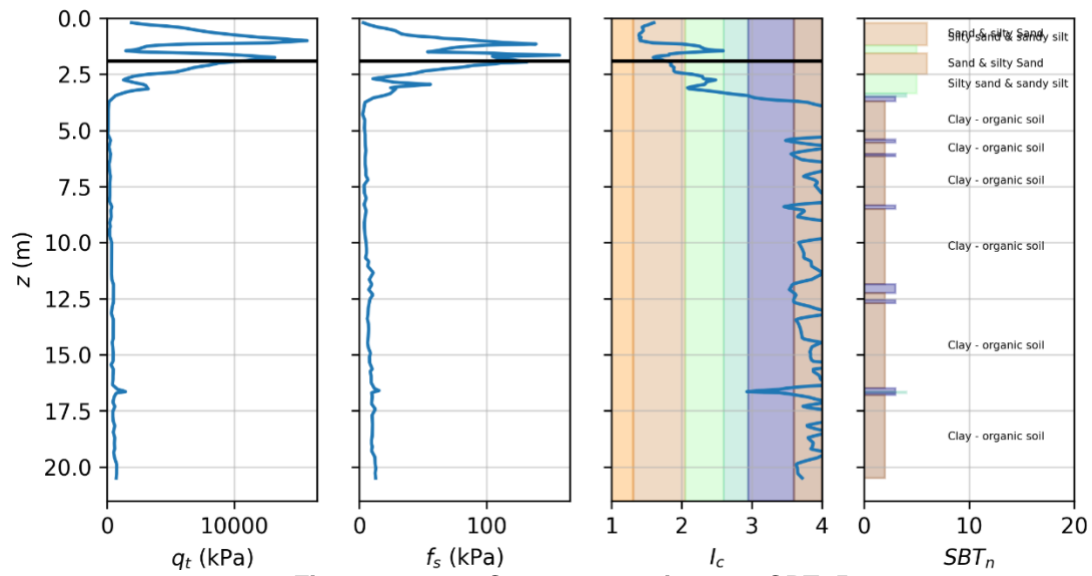


Figure 2.8 Cone penetration test CPT05.

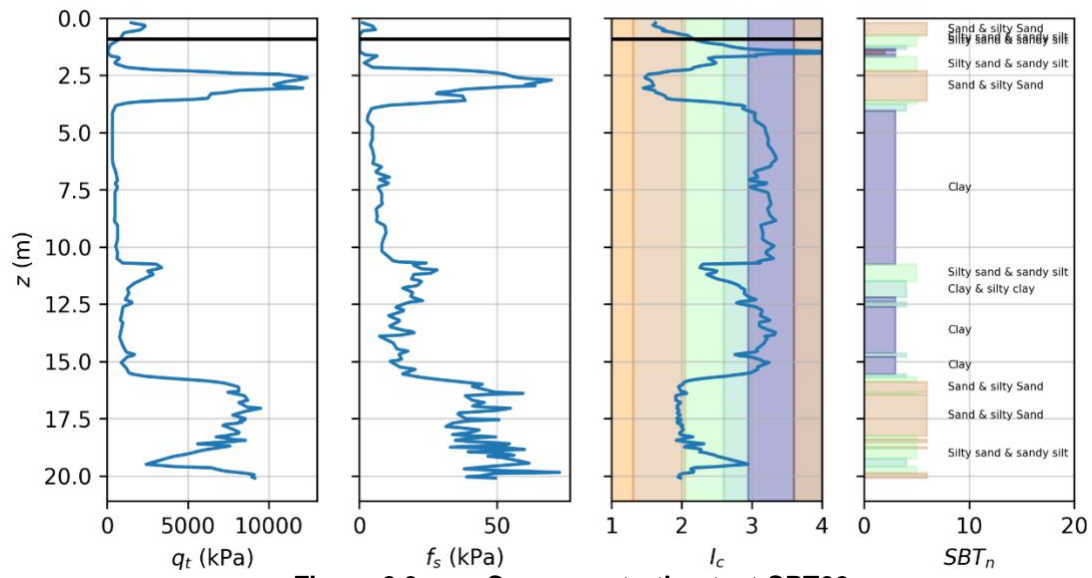


Figure 2.9 Cone penetration test CPT06.

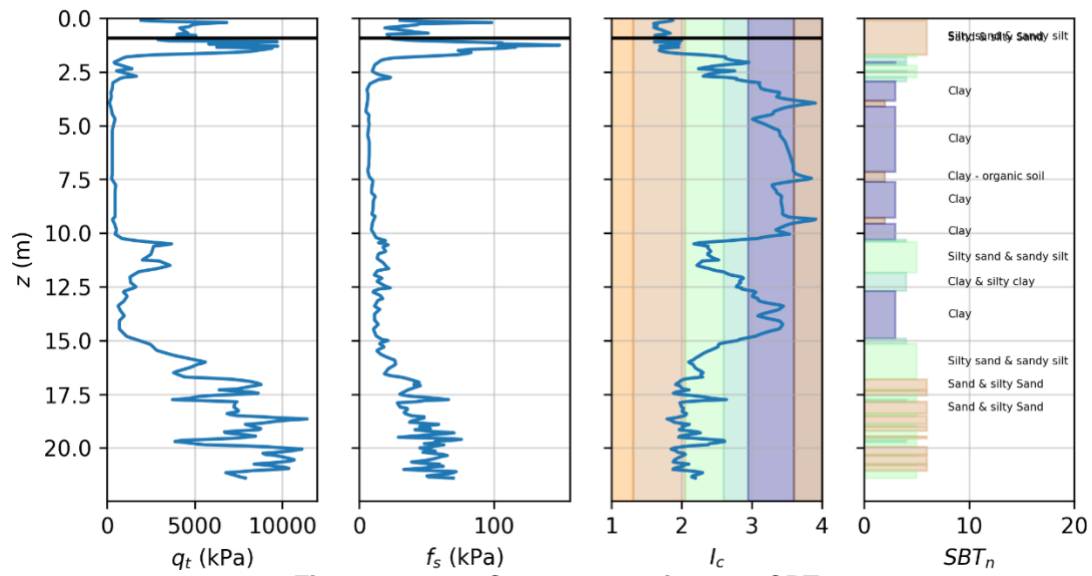


Figure 2.10 Cone penetration test CPT07.

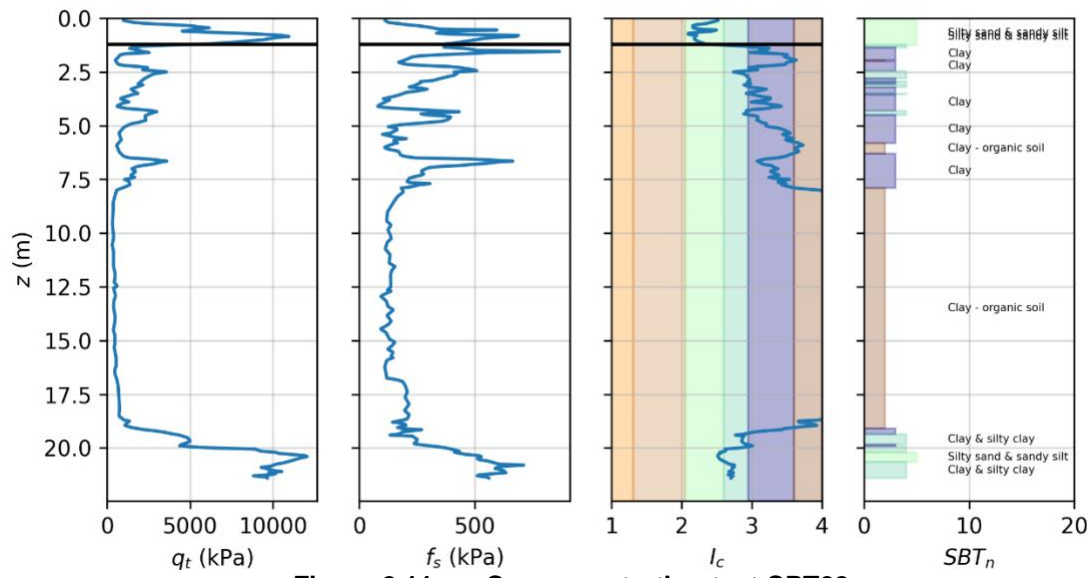


Figure 2.11 Cone penetration test CPT08.

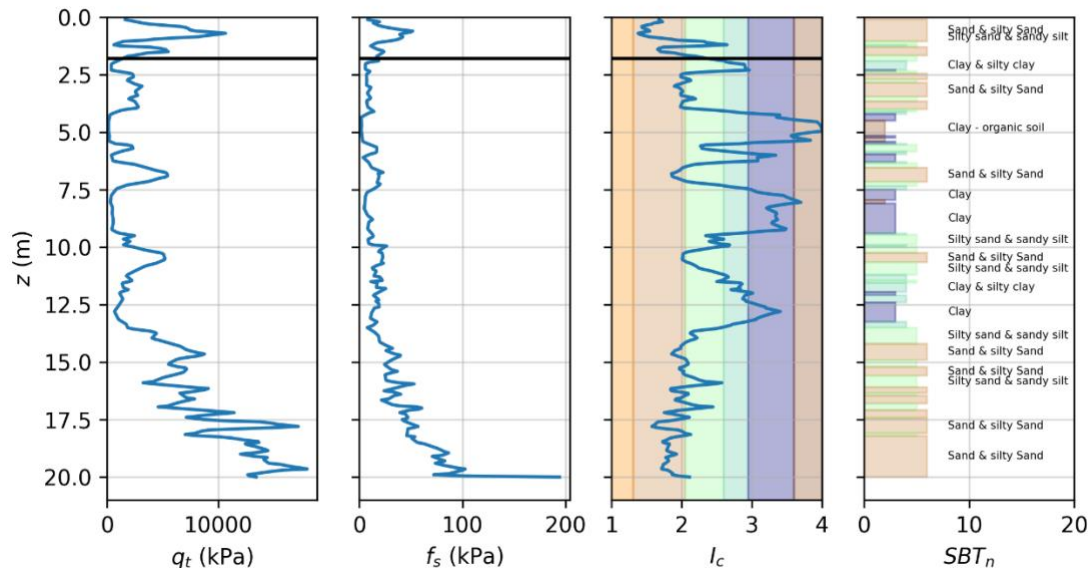


Figure 2.12 Cone penetration test CPT09.

Cross-sections interpreted from the CPT data are presented in Figs. 2.13 (A-A' in Fig. 2.3) and 2.14 (B-B' in Fig. 2.3). Plots of cone tip resistance are included to facilitate identification of stratigraphic contacts between the surface soil and hydraulic fill, and between the hydraulic fill and underlying alluvium. Although scales are not included on the cone tip resistance values, they are all scaled by the same amount to facilitate direct comparisons. The hydraulic fill layer is anticipated to be the culprit of surface evidence of liquefaction, so we focus our attention here on that layer. By combining Fig. 2.13 with more detailed information from each CPT in Figs. 2.4 to 2.9, we observe the following:

1. CPT01 and CPT02 contain relatively thick sandy layers and relatively weak surficial soil crust layers.
2. CPT03 consists of fine-grained soil with low tip resistance identified as silty sand / sandy silt overlying clay based on the *SBT_n* classification.
3. CPT04 contains sandy hydraulic fill and a strong surficial crust layer. The presence of sand at this location is inconsistent with expectations based on the position of the discharge pipe. It's possible that another discharge pipe was located near CPT04.
4. CPT05 and CPT06 contain clayey soils with very low tip resistance within the hydraulic fill layer.

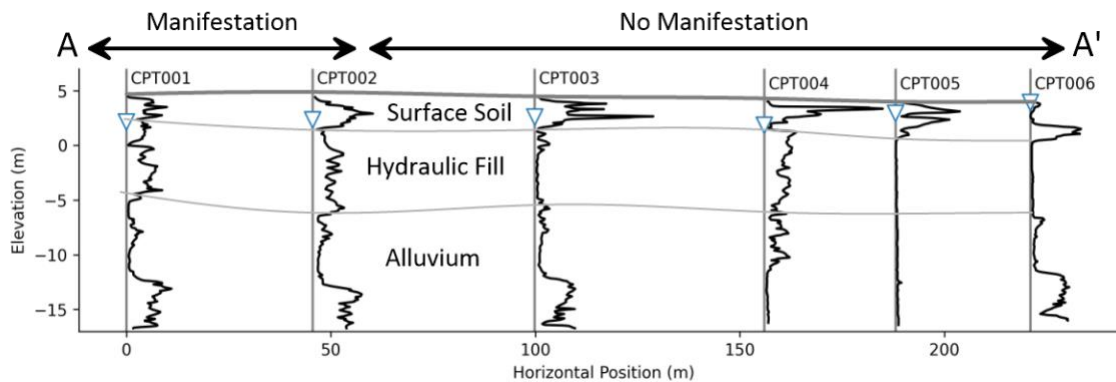


Figure 2.13 Cross-section interpreted from CPT test data along transect A-A' from Fig. 2.3.

Similarly, the following conclusions are drawn about cross-section B-B':

1. CPT06 and CPT07 consist of plastic clayey soils with very low tip resistance.
2. CPT08 consists of interbedded silt and clay layers within the hydraulic fill.
3. CPT09 has interbedded sandy and clayey soils within the hydraulic fill, and a relatively weak and thin crust layer.

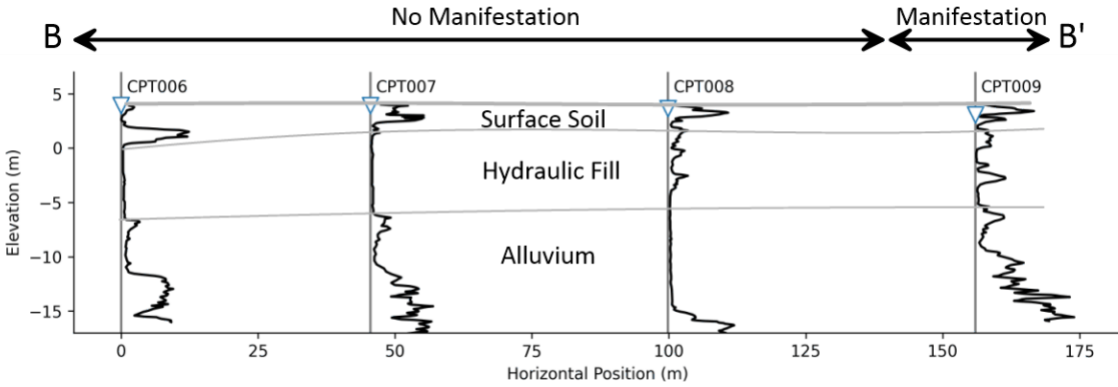


Figure 2.14 Cross-section interpreted from CPT test data along transect B-B from Fig. 2.3.

2.3 BORING LOGS

Three borings, B1, B3, and B6, are presented herein using the hatch legend in Fig. 2.15 to illustrate the depth variations of soil type. Boring logs for B1, B3, and B6 are presented in Figures 2.16 through 2.18. These boring logs are collocated with CPT001, CPT003, and CPT006, respectively. The rotary wash method was used to advance the boreholes, and the borehole diameter was 0.15m. Borings were performed by Jibanshikenjo Co. Ltd. in August 2015. The boring logs terminate near the bottom of the hydraulic fill, at shallower depths than the CPT's, because those soils were deemed more important to sample and test for the purpose of assessing liquefaction susceptibility and manifestation. In each case, the boring log confirms the soil types inferred from the cone penetration tests within the surface soil and hydraulic fill.

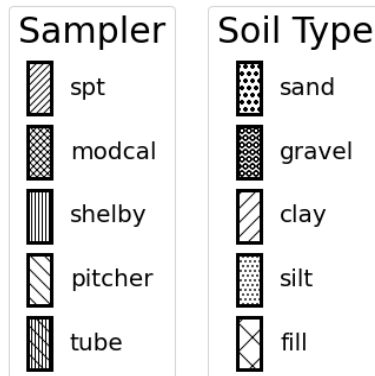


Figure 2.15 Boring log hatch legend.

Boring B1 consists of sandy soils to a depth of 8m, where the soil type transitions to silt. The fines content of the sand ranges from 5% to 28%, and natural water contents ranging from 35% to 40%. These water contents were measured using a triple tube sampler with an inner diameter of 70mm

and outer diameter of 73mm. Two SPT blow counts measured in the sand were both 9, and an SPT blow count in the silt was 2. This boring log confirms that soils at this location are susceptible to liquefaction and loose. The observations of surface manifestation at this location are therefore unsurprising.

Boring B3 consists of silty sand to a depth near 3.5 m overlying a layer of sand overlying silt. Fines content in the silty sand is 42%, and in the sand the fines content ranges from 1% to 8%. Water content in the silty sand is 50%, and in the sand the water content ranges from 32% to 34%. The SPT blow count in the silty sand layer is 2, and in the sandy silt is 3. Atterberg limits testing performed on the silty sand at a depth near 3m identified the liquid limit is 17% and the plastic limit could not be measured because the soil is non-plastic. The plastic limit is reported as 0 in the boring log because the NGL database currently only accepts numbers in the plastic limit field (i.e., the string “NP” or “non-plastic” is not allowed). We therefore consider these sandy soils to be susceptible to liquefaction. This site consists of soils that are susceptible to liquefaction and loose, yet surface manifestation was not observed at this location. We subsequently demonstrate that this site produces a false-negative prediction by available liquefaction triggering models.

Boring B6 consists of a sandy crust layer overlying clay. The sand is loose, and partially submerged below groundwater (note that two separate groundwater elevations were reported in the boring log). Laboratory triaxial and consolidation tests were performed on samples from the triple tube sampler (sample S-1), as reported in the next section. This site did not exhibit surface manifestation of liquefaction. The upper sand layer is susceptible, loose, and below the water table, but is also relatively thin. Lack of manifestation at this site may be explained in part by the thinness of the sand layer and the predominance of clay over most of the hydraulic fill thickness compared with the nearby sites that manifested liquefaction.

Site Name:	<u>Mihama-ward (8 Chome Meeting Place)</u>	Borehole Type:	<u>Rotary wash</u>
Surface Geology:	<u>Fill</u>	Drill Rig:	<u>Rotary wash</u>
Test Name:	<u>B1</u>	Crew:	<u>TK and IY - Jibanshikenio Co., Ltd.</u>
Latitude:	<u>35.6317</u>	Borehole Diameter (m):	<u>0.15</u>
Longitude:	<u>140.05169</u>	Hammer Type:	<u>Automatic hammer release / 63.5kg Donut hammer</u>
Start Date:	<u>2015-08-10 00:00:00</u>	Borehole Method:	
Remarks:			

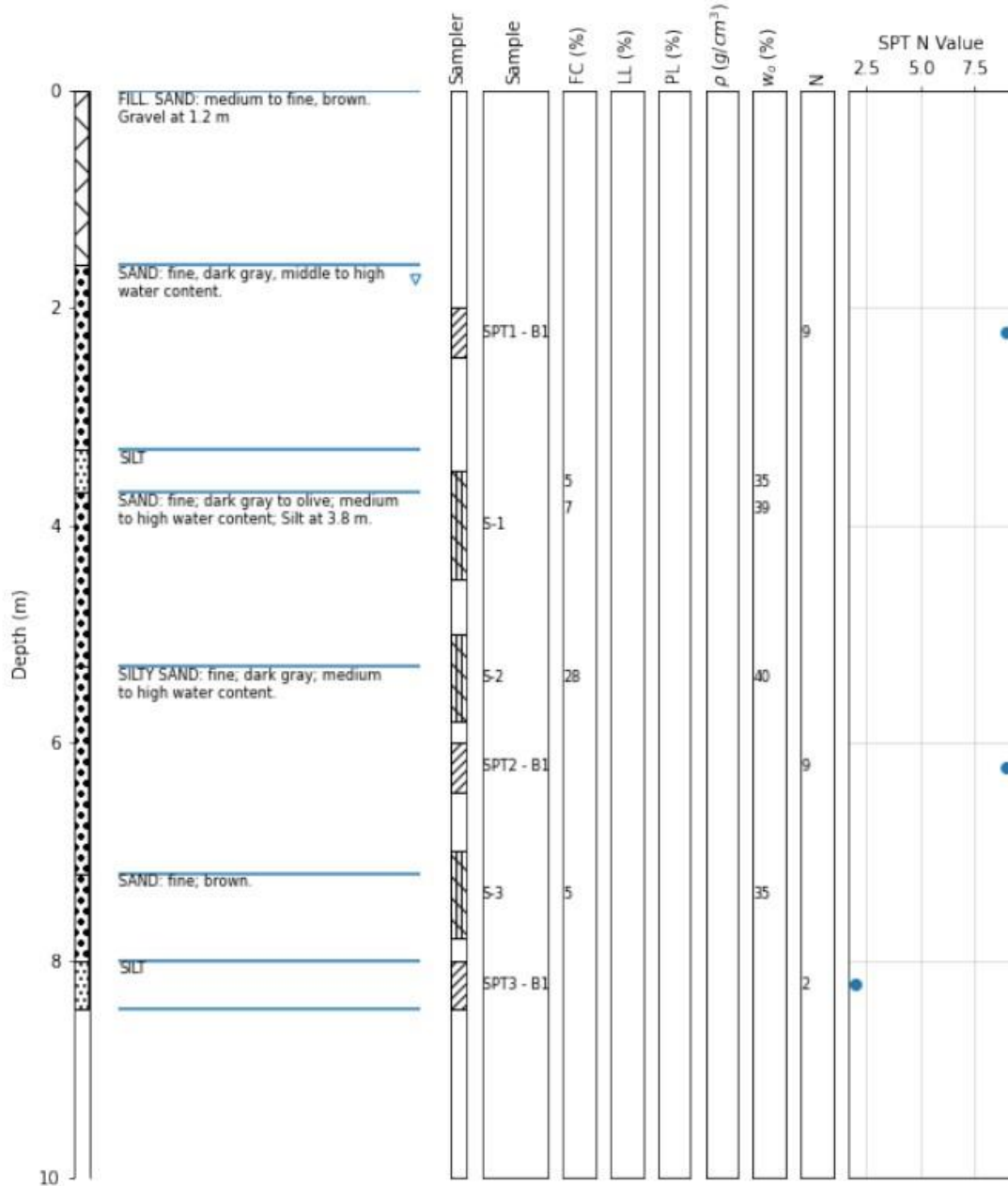


Figure 2.16 Boring log for B1.

Site Name:	<u>Mihama-ward (8 Chome Meeting Place)</u>	Borehole Type:	<u>Rotary wash</u>
Surface Geology:	<u>Fill</u>	Drill Rig:	<u>Rotary wash</u>
Test Name:	<u>B3</u>	Crew:	<u>TK and IY - Jibanshikenjo Co., Ltd.</u>
Latitude:	<u>35.6399</u>	Borehole Diameter (m):	<u>0.15</u>
Longitude:	<u>140.05277</u>	Hammer Type:	<u>Automatic hammer release / 63.5kg Donut hammer</u>
Start Date:	<u>2015-08-11 00:00:00</u>	Borehole Method:	
Remarks:			

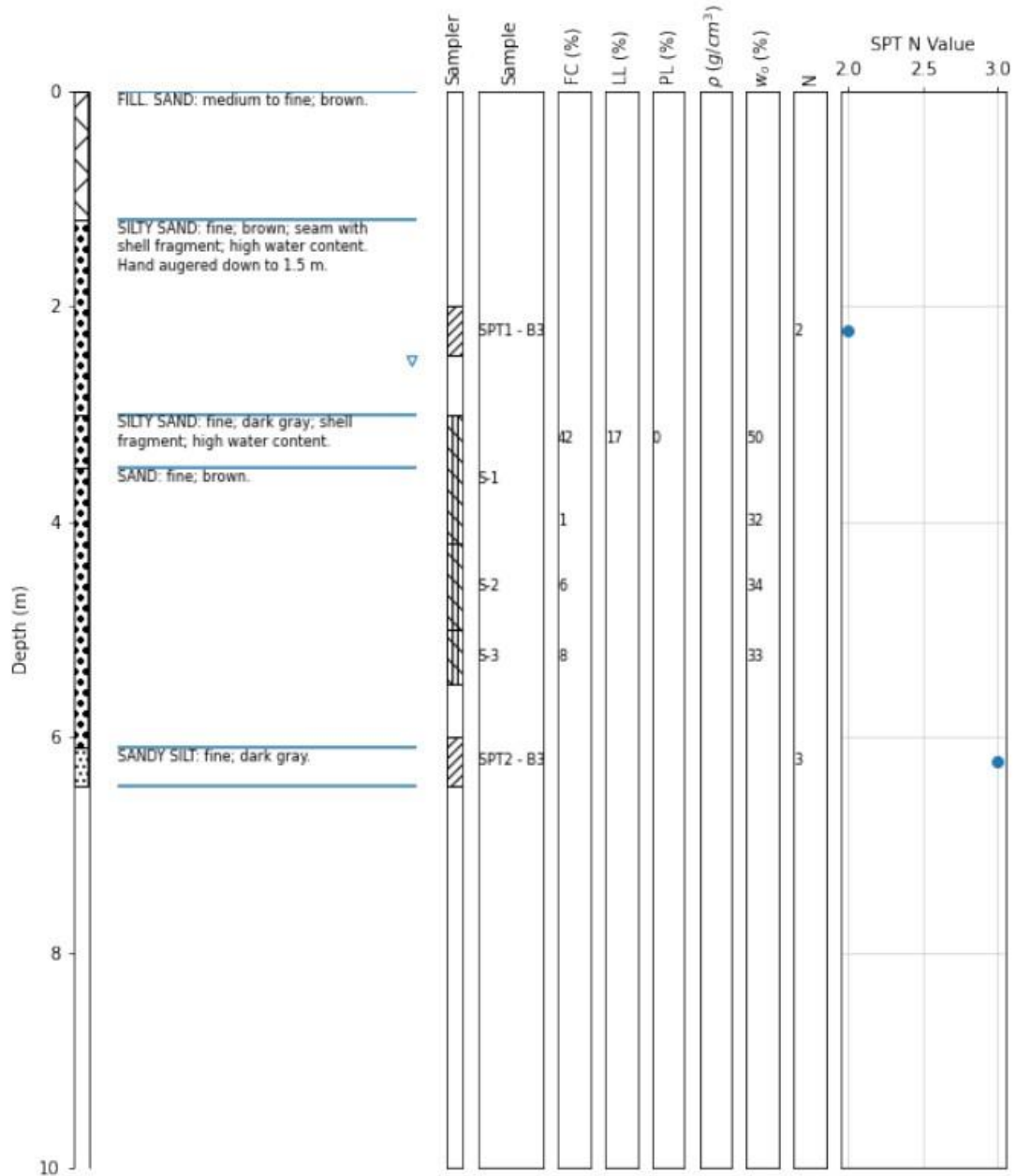


Figure 2.17 Boring log for B3.

Site Name:	<u>Mihama-ward (8 Chome Meeting Place)</u>	Borehole Type:	<u>Rotary wash</u>
Surface Geology:	<u>Fill</u>	Drill Rig:	<u>Rotary wash</u>
Test Name:	<u>B6</u>	Crew:	<u>TK and IY - Jibanshikenjo Co., Ltd.</u>
Latitude:	<u>35.630243</u>	Borehole Diameter (m):	<u>0.15</u>
Longitude:	<u>140.053657</u>	Hammer Type:	<u>Automatic hammer release / 63.5kg Donut hammer</u>
Start Date:	<u>2015-07-27 00:00:00</u>	Borehole Method:	
Remarks:			

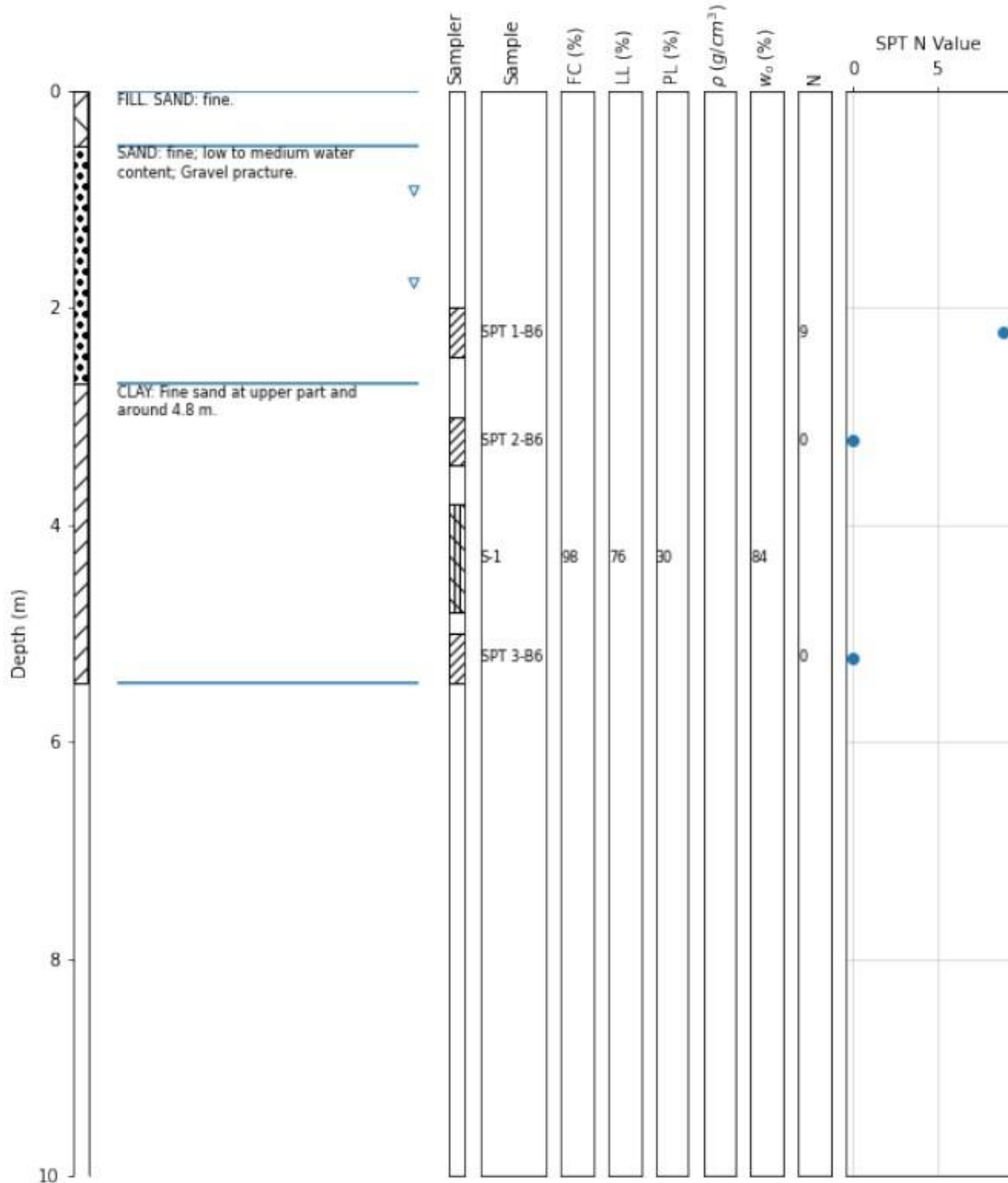


Figure 2.18 Boring log for B6.

2.4 TRIAXIAL TESTS

A set of monotonic consolidated undrained triaxial compression tests were performed by Tokyo Soils, Inc. for specimens trimmed from Boring 1, Samples S-2 and S-3, and from Boring 6, Sample S-1. Three loading stages were imposed on each specimen in which the specimen was sheared to failure. Each stage involved progressively higher reconsolidation stress. Results from those tests are provided in Appendix A, and are included in the NGL database. We initially anticipated performing cyclic tests of these soils in the UCLA Advanced Geotechnical Testing laboratory because we had anticipated that the Mihama Ward case history would elucidate aspects of liquefaction susceptibility that could be observed on disturbed specimens. However, susceptibility was found to be a non-issue. For this reason, we opted not to conduct a cyclic laboratory testing program because (i) we would be unable to reconstitute the sand specimens to their in-situ density and fabric, and (ii) cyclic softening of the clayey soils was not an issue. Nevertheless, the laboratory tests performed by Tokyo Soil, Inc. are included in this report for completeness.

2.5 LIQUEFACTION TRIGGERING EVALUATION

Liquefaction triggering evaluations were performed using the legacy CPT procedure by Boulanger and Idriss (2016). We utilize the boring logs to inform selection of soil type, and for fines corrections to the CPT data, but we did not perform an SPT-based triggering evaluation because we consider the blow counts to be too infrequent to adequately capture distributions of penetration resistance in potentially liquefiable materials. The peak acceleration at the site was computed by interpolating within-event residuals from nearby recorded ground motion records using ordinary Kriging as described by Kwak et al. (2011). Variogram models utilized in the Kriging interpolation were developed by Pretell et al. (2024) using a Bayesian inference method involving Markov-Chain Monte Carlo simulations, following the method by [Bodenmann et al. \(2023\)](#). The PGA at the site was interpolated to be 0.203g, with a standard deviation of the natural logarithm of the interpolation error being 0.246.

The liquefaction triggering procedures utilized herein were developed by first selecting a critical layer, and subsequently plotting its corrected penetration resistance vs. corrected cyclic stress ratio. However, they are often not applied in that manner in practice. Rather than pre-selecting a critical layer, we compute CSR and CRR for each data point in the CPT profiles. We then make inferences about liquefaction manifestation based on those plots. The results are provided in Figs. 2.19 through 2.27 for the CPT data. Lines for *CRR* and *FS_L* are plotted only for soils where $I_c < 2.8$, and $z > z_{gwt}$. Often a lower susceptibility threshold of $I_c < 2.6$ is applied to CPT data. However, we adjusted it up in this case based on Atterberg limits tests from B3 that indicated the silty materials are non-plastic, and have I_c between 2.6 and 2.8.

These figures support the following conclusions:

1. CPT's where manifestations were observed (i.e., CPT001, 002, and 009) all have significant continuous thicknesses of soil with $FS_L < 1.0$ immediately below the groundwater table. The triggering procedure accurately predicts manifestations at these sites, which are considered true positives.
2. CPT004 is similar to CPT001, 002, and 009 in that it also has a layer of significant thickness immediately below the water table with $FS_L < 1.0$. Therefore, manifestation would be anticipated for this profile. However, manifestation was not observed. This case is therefore a false positive. The most notable differences between CPT004 and the three that manifested are (i) CPT004 exhibits a gradual fining sequence in the sand layer immediately beneath the groundwater table, whereas the other CPT's do not, and (ii) the crust layer above the water table has significantly higher q_{c1Ncs} than the others. Our interpretation is that liquefaction likely triggered in this profile, but manifestations were suppressed by the crust.
3. CPT003, 005, 006, and 007 all contain layers that have $FS_L < 1.0$ at depths immediately below the groundwater table. Furthermore, CPT003, 006, and 007 all have layers near the bottom of the profile, at depths generally larger than 17m, with $FS_L < 1.0$. None of these profiles manifested liquefaction, so these are considered false positives. However, the shallow layers with $FS_L < 1.0$ are thin, and interbedded with fine-grained soils. Interbedded soils have recently been observed to produce false positives for sites in Christchurch, New Zealand (e.g., (Cubrinovski et al. 2019)). It is unclear whether these layers triggered and did not manifest because they are thin and sandwiched between fine-grained layers, or whether they did not trigger. Additionally, the thicker more continuous layers at depths larger than 17m are likely to have triggered, but not manifested at the surface given their large depth. The extent to which these deep layers may have contributed to surface settlement is unclear. But they did not produce sand boils, or other surface manifestations apparent during reconnaissance.
4. CPT008 consists of clayey layers throughout most of the profile. The sand layer at a depth of 20m is dense, and has $FS_L > 1.0$. We therefore consider this case to be a true negative.

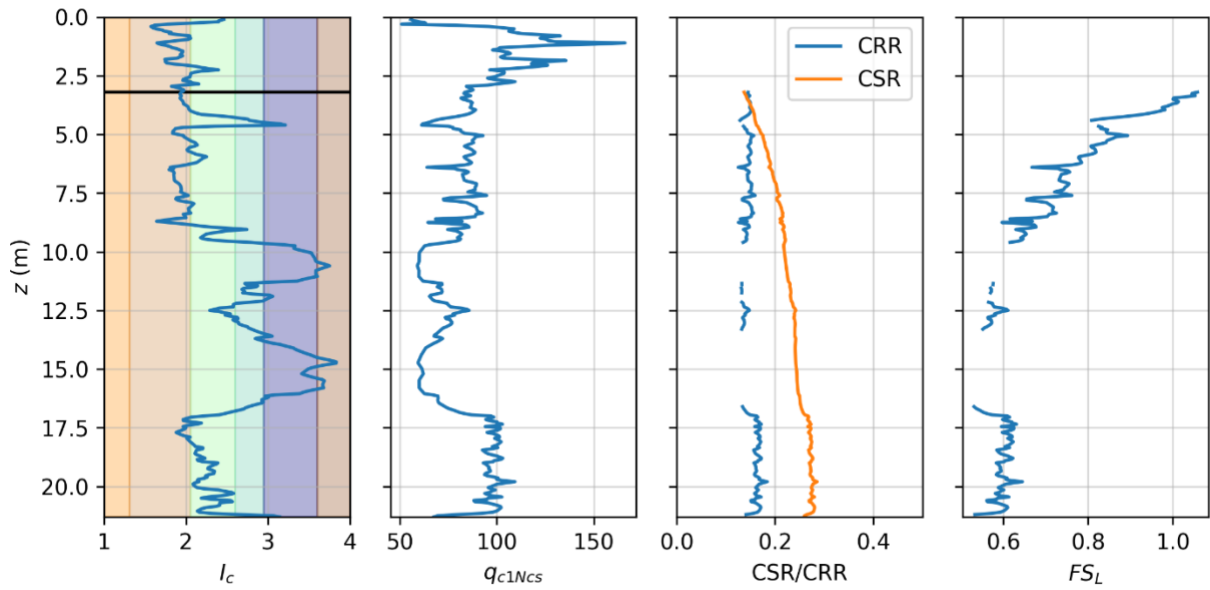


Figure 2.19 Liquefaction triggering evaluation of CPT001 (manifestation = yes).

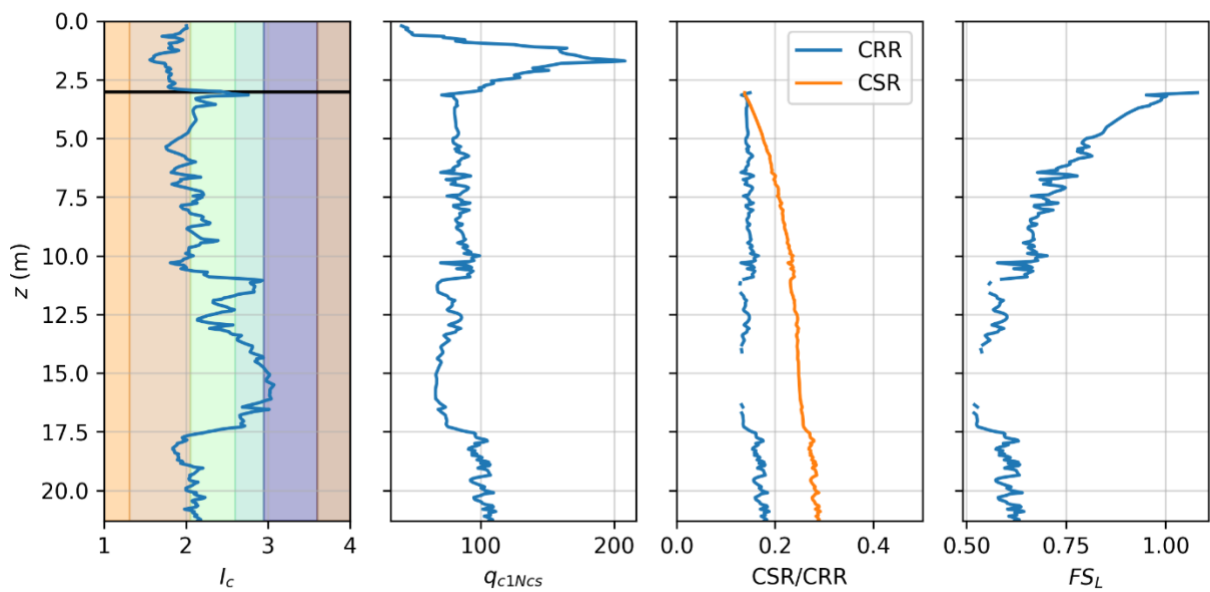


Figure 2.20 Liquefaction triggering evaluation of CPT002 (manifestation = yes).

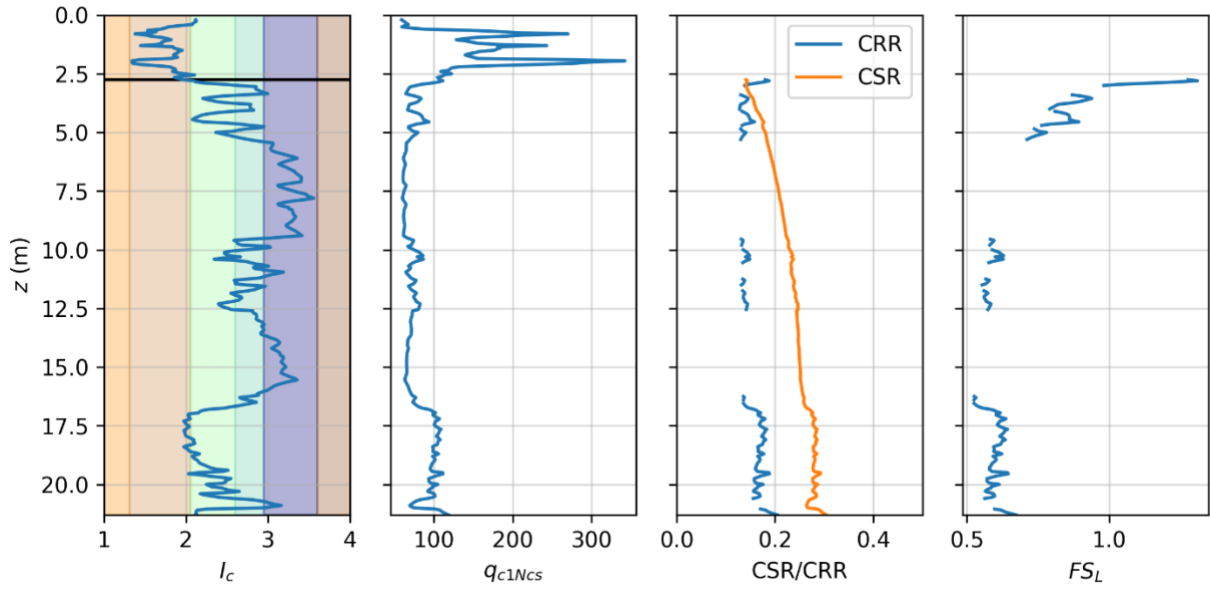


Figure 2.21 Liquefaction triggering evaluation of CPT003 (manifestation = no).

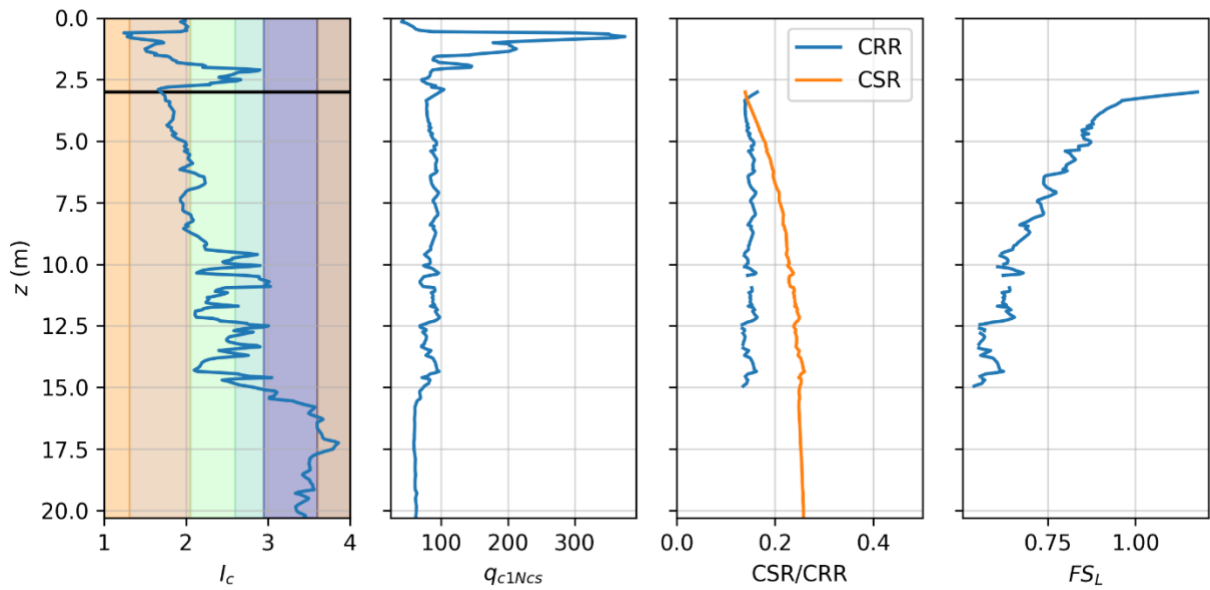


Figure 2.22 Liquefaction triggering evaluation of CPT004 (manifestation = no).

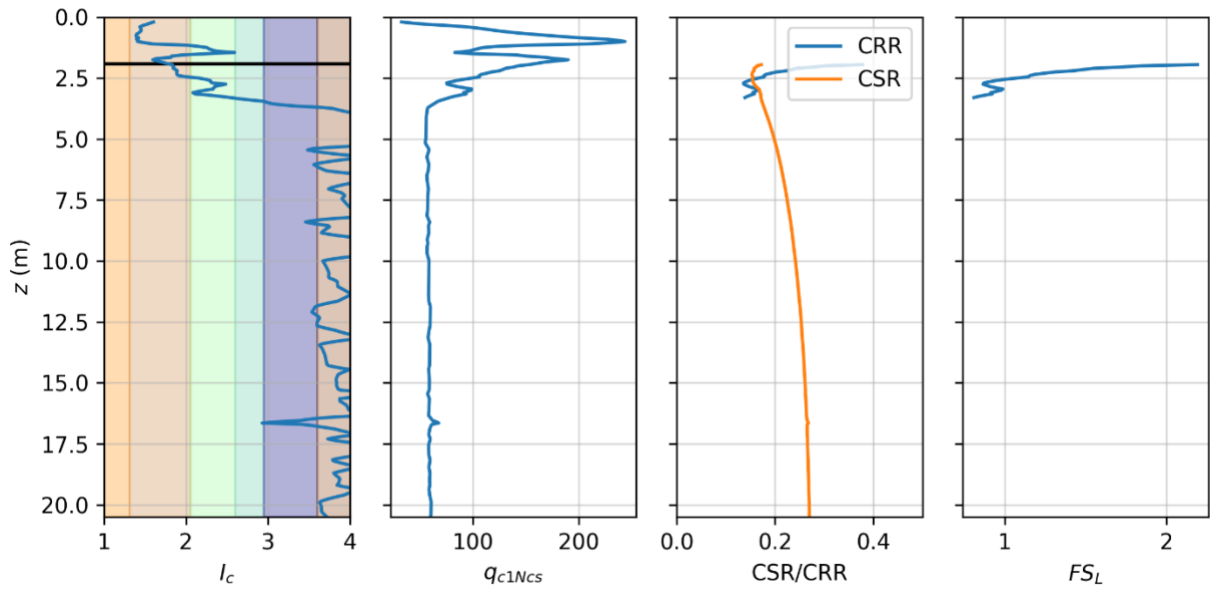


Figure 2.23 Liquefaction triggering evaluation of CPT005 (manifestation = no).

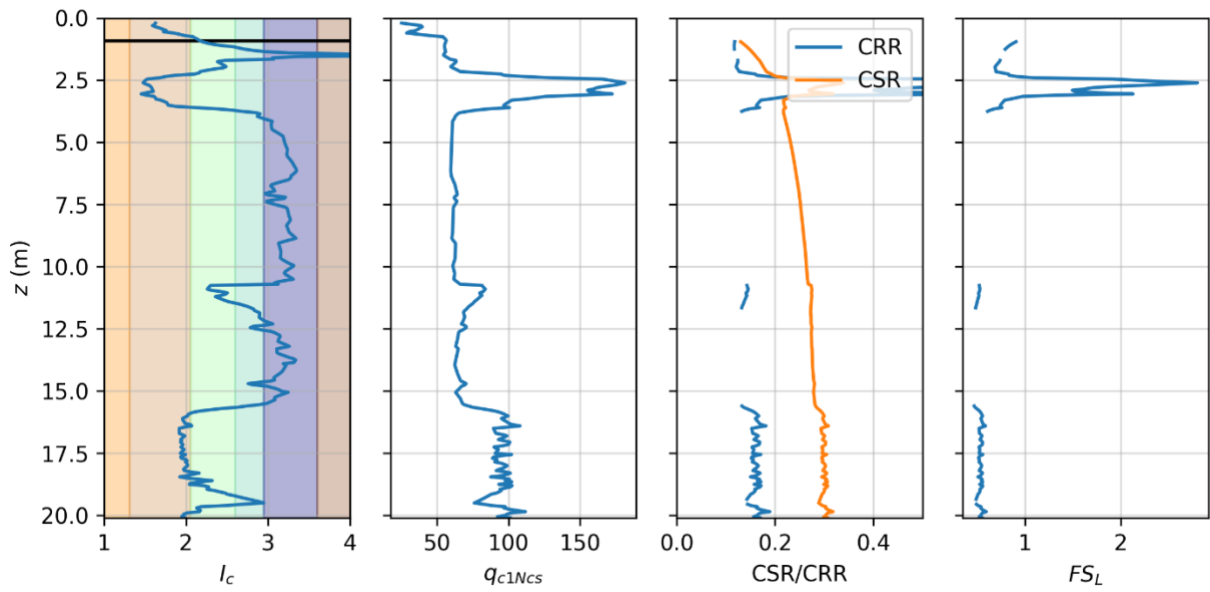


Figure 2.24 Liquefaction triggering evaluation of CPT006 (manifestation = no).

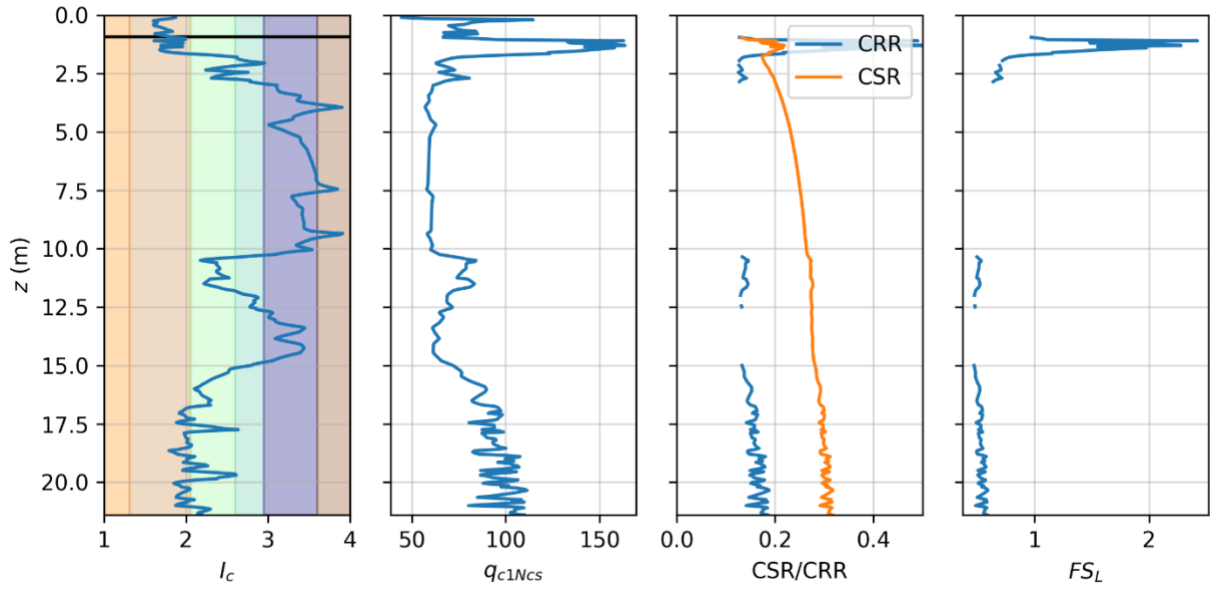


Figure 2.25 Liquefaction triggering evaluation of CPT007 (manifestation = no).

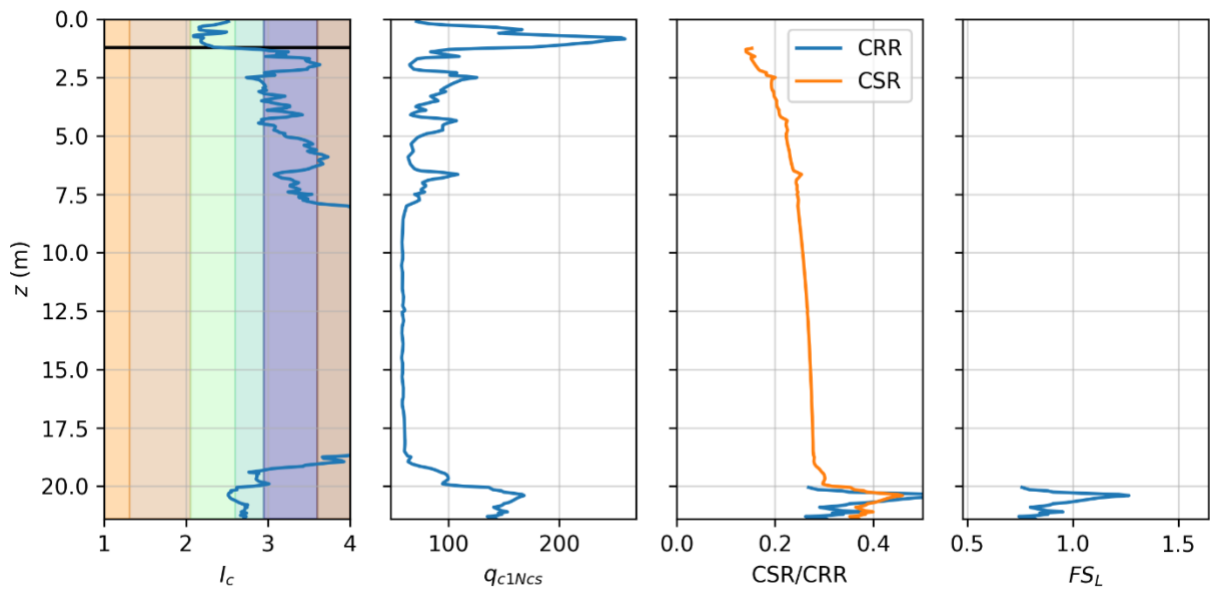


Figure 2.26 Liquefaction triggering evaluation of CPT008 (manifestation = no).

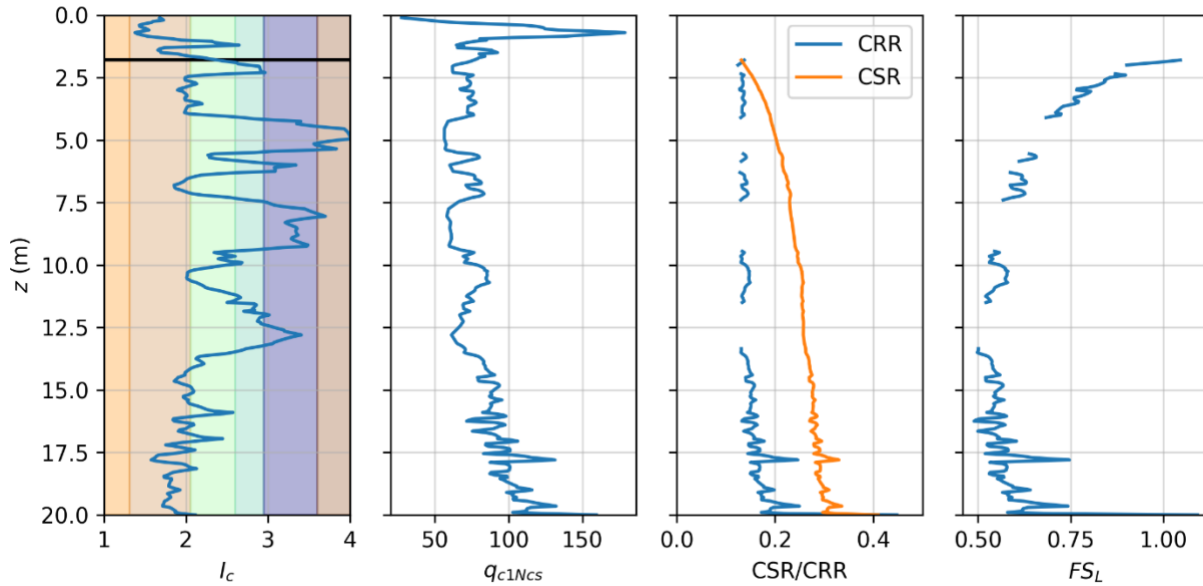


Figure 2.27 Liquefaction triggering evaluation of CPT009 (manifestation = yes).

Having interpreted the profiles, we now turn our attention to critical layer assignment for comparison with the Boulanger and Idriss (2016) triggering relationship. Assigning critical layers to these CPT profiles for the purpose of plotting a single point on the triggering curve requires judgment. Many different layers might contribute to manifestations, and selecting one single layer to be representative of the profile is subjective, and would likely be done differently by different people. For example, some analysts might select the layer with the lowest factor of safety, even if it is deep and/or thin, and other layers with higher FS_L that are thicker and/or shallower. In this case, our judgment focused on how likely a layer is to manifest liquefaction. We therefore favor shallow layers over deeper layers, thicker layers over thinner layers, and looser layers over denser layers, and apply judgment when balancing these criteria. Our selections are summarized in Table 2.1, and plotted in Fig. 2.28 along with the Boulanger and Idriss (2016) triggering curves for probabilities of 15, 50, and 85%. The “yes” points all plot above the 50% triggering curve, and are considered true positives. All but one of the “no” points also plot above the 50% triggering curve, and are therefore considered false positives. Furthermore, the “yes” and “no” data points are not separable in $q_{c1Ncs} - CSR$ space. This indicates that other variables, such as layer thickness, plasticity, fines content, and/or depth, may contribute to manifestation.

Table 2-1 Critical layer properties for CPT triggering evaluation.

CPT	z_{top} (m)	z_{bot} (m)	q_{c1Ncs}	CSR
CPT001	3.1	9.6	90	0.18
CPT002	3.0	14.0	85	0.20
CPT003	3.4	5.3	76	0.17
CPT004	3.0	10.0	90	0.20
CPT005	2.5	3.4	88	0.15
CPT006	15.5	19.5	78	0.28
CPT007	10.4	12.0	78	0.27
CPT008	20.0	21.2	146	0.40
CPT009	9.5	11.5	82	0.25

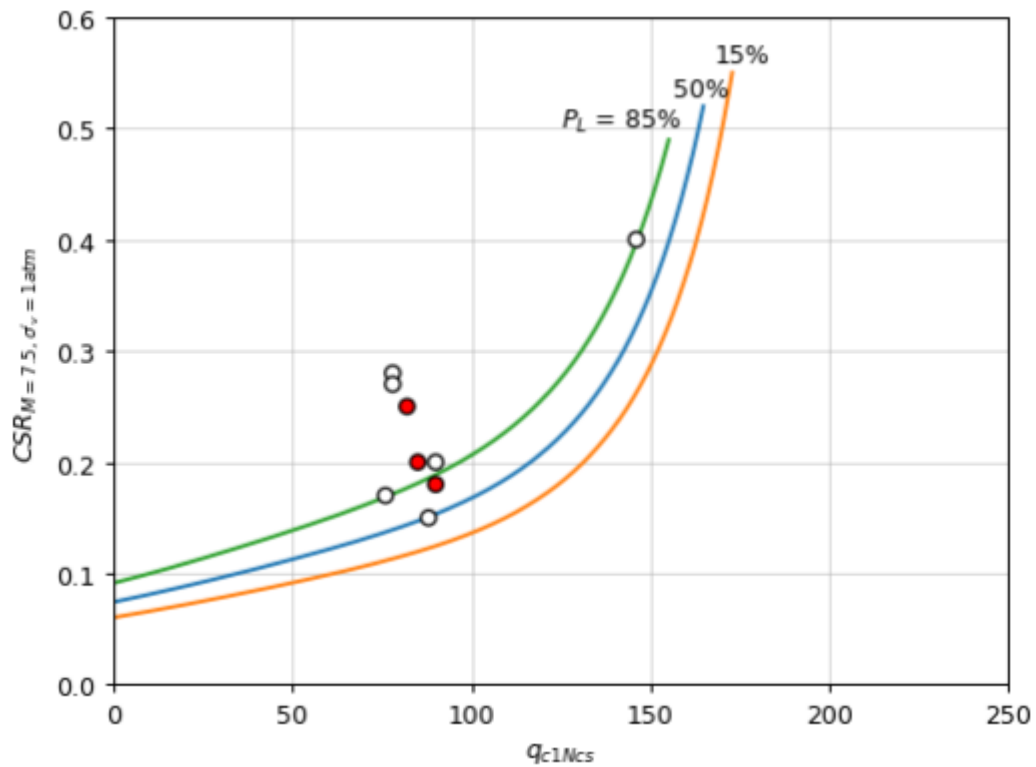


Figure 2.28 Critical layer selections plotted along with Boulanger and Idriss (2016) triggering curves. Open circles are manifestation = no, closed circles are manifestation = yes.

3 LABORATORY SCHEMA FOR NGL DATABASE

The Next Generation Liquefaction (NGL) database (Ulmer et al. 2023) was originally configured to store field test data, such as cone penetration tests, boring logs, and geophysical tests, alongside observation data about ground failure or lack thereof from past earthquake events. The original database had some laboratory test data involving index tests, such as grain size distributions and Atterberg limits. As part of this study, the laboratory component of the NGL database was expanded to include direct simple shear tests, triaxial tests, and consolidation tests. As described earlier, data of this type is useful for engineering assessments of liquefaction susceptibility.

3.1 LABORATORY DATABASE SCHEMA

The schema for the laboratory component is presented in Fig. 3.1. Many components of the NGL schema are omitted from Fig. 3.1 for brevity and clarity, but the rest of the NGL schema, including the field data, earthquake data, and observation data can be found at <http://nextgenerationliquefaction.org/schema/index.html> and (Hudson et al. 2022).

The highest level table for the laboratory component is the “LAB” table, which contains a primary key “LAB_ID” along with the name, location, and description of the lab. The next table in the hierarchy is the “LAB_PROGRAM” table, which contains a primary key “LAB_PROGRAM_ID” and a foreign key “LAB_ID” to establish a relationship between the laboratory testing program and the laboratory where it was performed. A single laboratory may have many different lab testing programs. Any NGL users associated with a lab testing program are linked via a junction table called “LAB_PROGRAM_USER”, which contains only a primary key, a foreign key for the “LAB_PROGRAM” table and a foreign key for the “USER” table. The purpose of a junction table is to enable a “one-to-many” relationship in which many users may be associated with a single lab testing program. Similarly, samples are associated with a laboratory testing program through the “LAB_PROGRAM_SAMPLE” junction table. A sample can either be created in a laboratory (e.g., by blending and hydrating clay minerals) or it can come from a field testing program. If a sample comes from a field testing program, the “SAMP_TEST” junction table establishes a relationship between the sample and field test from which it came.

A specimen tested in a laboratory device is described by the “SPEC” table, which contains a foreign key to the sample table. The “SPEC_ID” field is then a foreign key for a series of possible laboratory tests that could be performed, including grain size distribution, plasticity, various index tests, density measurements, consolidation, triaxial, direct simple shear, and “others” for any tests that were not captured in this list. The tables “Relative Density”, “Atterberg Limits”, and “Index Tests” contain information about these tests within a single table. By contrast, the triaxial, direct simple shear, and consolidation laboratory tests are more complicated and involve stages that must

be fully documented. To provide this documentation, each of these tests has a general table, a stages table, and a data table. The general tables (TXG, DSSG, and CONG, for triaxial, direct simple shear, and consolidation, respectively) contain test-specific information about the specimen including initial void ratio, initial water content, diameter, height, and a specimen description. Information about loading stages are then entered into the appropriate stage tables (TXS, DSSS, CON_STGE for triaxial, direct simple shear, and consolidation, respectively) that contain a foreign key from the appropriate general table, and data arising from these load stages are entered into appropriate data tables (TXD, DSSD1D, DSSD2D, COND for triaxial, one-dimensional direct simple shear, two-dimensional direct simple shear, and consolidation, respectively), which contain the appropriate load stage ID as a foreign key.

As an example of the database structure, a direct simple shear test might consist of a consolidation stage in which the specimen is consolidated to a desired pressure, followed by a cyclic loading stage in which the specimen is cyclically sheared, followed by a post-cyclic reconsolidation stage. In this case, the test would have one entry in the SPEC table, one entry in the DSSG table, two entries in the DSSS table, and all of the data from each stage would be stored in many entries in the DSSD table. It is important to include data from all of these stages to track the evolution of the specimen response throughout the test. Measurements made during each stage are the same for a particular laboratory test. In some cases, a quantity remains constant during the test. For example, in a constant height direct simple shear test, the vertical strain field “DSSD1D_EPSV” would be anticipated to be constant. However, we believe it is important to measure the vertical strain to verify that constant height conditions were achieved, and these data should be included. Similarly shear stress and shear strain should be zero during the consolidation phase of a direct simple shear test (assuming the specimen is consolidated without a static shear bias), but these measurements are nevertheless required as part of documentation of the stage. Atterberg Limits tests and other simple tests may be performed on samples associated with more complicated lab tests, and can be linked by matching a SAMPLE_ID foreign key in the Atterberg Limits table with that in the general table for the more complicated lab test.

3.2 DATABASE POPULATION

3.2.1 Laboratories

Four laboratories have been entered into the NGL database (Table 3.1) that contain at least one triaxial, direct simple shear, or consolidation test. The laboratories are the University of Canterbury Geomechanics Laboratory, the UCLA Advanced Geotechnical Laboratory, the Tokyo Soil Research Co. Ltd. laboratory, and the Oregon State University Geotechnical Laboratory.

Table 3-1 Laboratories in NGL database (last accessed 07/15/2023).

LAB_ID	LAB_NAME	LAB_LAT (degrees)	LAB_LON (degrees)
1	University of Canterbury Geomechanics Laboratory	-43.5226	172.5794
2	UCLA Advanced Geotechnical Laboratory	34.0692	-118.4427
3	Tokyo Soil Research Co. Ltd.	36.0594	140.1427
9	Oregon State University Geotechnical Laboratory	44.5638	-123.2794

3.2.2 Laboratory Test Programs

The database currently contains nine laboratory testing programs performed at four different laboratories, as defined in Table 3.2. These testing programs include 1. a triaxial testing program performed on specimens of fine-grained soil obtained from field samples at the University of Canterbury Geomechanics Laboratory following the Canterbury earthquake sequence (Beyzaei 2017), 2. Cyclic and monotonic direct simple shear tests performed on samples of sand constructed in the UCLA Advanced Geotechnical Laboratory (Eslami 2017), 3, 4. Monotonic triaxial compression and consolidation tests performed at the Tokyo Soil Research Co. Ltd. laboratory on samples from Mihama ward with varying levels of liquefaction susceptibility (Tokyo Soils 2016), 5. Tests performed at UCLA on remolded samples from Mihama Ward, 6. Tests performed on fine-grained soils at the PDX Airport Test Site, 7. Tests performed on fine-grained soils at the Van Buren Bridge Test Site, 8. Tests performed on fine-grained soils at the Boone Bridge Site (Site F), and 9. Tests performed on fine-grained soils at the PDX-TS4 (Site E) location. Note that the

LAB_PROGRAM_ID contains some gaps. This is because a program may exist, but not have any associated triaxial, direct simple shear, or consolidation tests in the database. The number of tests performed as part of each test program are also indicated in Table 3.2.

Table 3-2 Laboratory test programs and number of tests in each program in NGL database.

LAB_PR OGRAM _ID	LAB _ID	LAB_PROGRAM_DESC	Number of Tests By Type						
			TXG	DSSG	CONG	GRAG	PLAS	RDEN	INDX
1	1	Testing of samples from sites associated with the Canterbury Earthquake Sequence (Beyzaei 2017)	42	0	0	56	38	6	35
2	2	Monotonic triaxial tests on Orange Co. Silica Sand (Eslami 2017)	14	0	0	0	0	0	0
3	3	Testing on samples from Mihama Ward associated with 2011 Tohoku earthquake (Tokyo Soils 2016)	7	0	0	0	0	0	7
7	2	Monotonic and Cyclic direct simple shear testing on clay-silt blends (Eslami 2017)	0	52	3	0	3	0	0
8	2	Testing of remolded samples from Mihama Ward (Eslami 2017)	0	0	1	0	0	0	0
11	9	PDX Airport Test Site	0	19	5	10	19	0	31
12	9	Van Buren Bridge Test Site	0	16	2	2	12	0	19
13	9	Boone Bridge Site (Site F)	0	25	3	2	9	0	19
14	9	PDX-TS4 (Site E)	0	41	6	7	41	0	79

3.3 ACCESSING THROUGH GRAPHICAL USER INTERFACE

The NGL database features a graphical user interface (GUI) at <https://nextgenerationliquefaction.org/> that displays field test data, earthquake event data, and observations at field sites following earthquakes. A screenshot of the GUI is shown in Fig. 3.2. The GUI currently does not display laboratory test data, but this feature is being developed as part of the broader NGL project organized through the Southwest Research Institute and will be released at a later date. We envision that a toggle switch will be added to the “General description” field in the toolbar on the right that will enable users to click on and off the location of laboratories. Clicking on a laboratory icon will bring up a menu of the test programs associated with that laboratory. Users will then be able to select a test program and view/download data from laboratory tests associated with that program in the GUI.

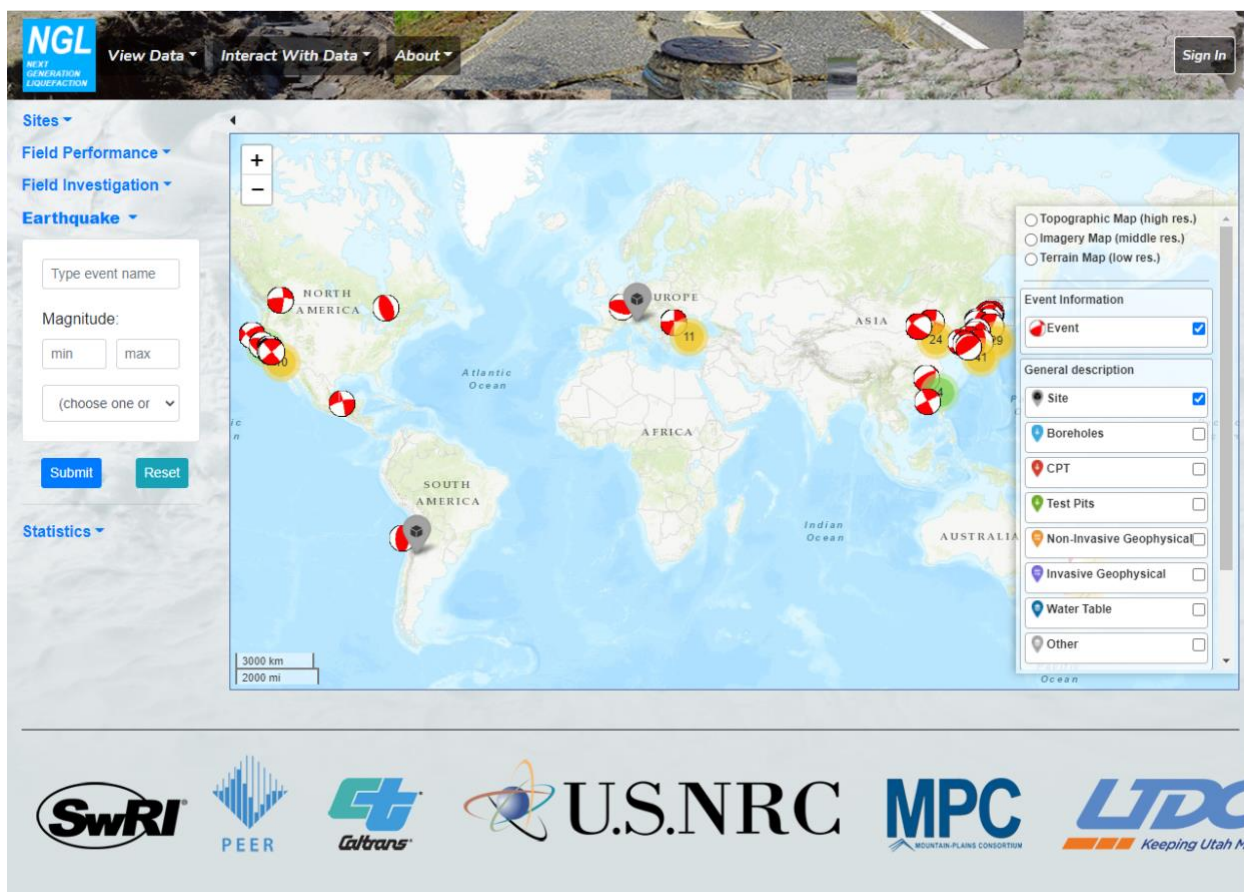


Figure 3.2 Next generation liquefaction graphical user interface. <https://nextgenerationliquefaction.org/> accessed 07/15/2023.

3.4 INTERACTING WITH DATA IN DESIGNSAFE

The GUI enables users to view or download data from a particular test program, but we envision that users may want to do more with the data than we can reasonably enable through a web interface. For this reason, the NGL database is replicated daily to DesignSafe (Rathje et al. 2017). The DesignSafe copy of the database can be accessed by users via Python scripts in Jupyter notebooks using the *pymysql* package. Figure 3.3 is an example Jupyter notebook used to query the data presented in Table 3.2. The first 3 lines are import statements for the *pymysql*, *numpy*, and *pandas* packages used in the script. Line 4 connects to the database using credentials defined in the previous cell and omitted from Fig. 3.3 for security. Line 5 defines a cursor used to query the database. Line 7 defines the types of tests we are interested in querying, and line 8 defines a Python dictionary called “output” where data are stored. Line 10 is a SQL query that obtains the LAB_PROGRAM_ID, LAB_ID, and LAB_PROGRAM_DESC fields from the LAB_PROGRAM database, and sorts them in ascending order by LAB_PROGRAM_ID. Line 11 executes the query, and line 12 fetches data generated by the query. Lines 13 through 15 initialize arrays into which the LAB_PROGRAM_ID, LAB_ID, and LAB_PROGRAM_DESC fields are stored, and lines 16 through 19 populates these fields using a “for” loop. Lines 20 to 22 place these arrays into the output dictionary. Lines 24 through 31 query the database to count the number of different types of tests for each test type, and for each value of the LAB_PROGRAM_ID field, values are appended to the appropriate column in the output field. Finally, the output field is placed into a Pandas dataframe and displayed in the output field.

The query defined in lines 26 through 28 warrants further discussion. In this case, we use the “COUNT” function in SQL to sum the number of fields that meet a particular condition. On line 26, the command “+ t + ‘.’ + t + ‘_ID)” will take the current value of the test_type list, and use it to generate the appropriate quantity to query. For example, for test_type = ‘TXG’ and lab_program_id = 1, the SQL query would be as follows: “SELECT COUNT TXG.TXG_ID FROM SAMP INNER JOIN LAB_PROGRAM_SAMP ON SAMP.SAMP_ID = LAB_PROGRAM_SAMP.SAMP_ID INNER JOIN SPEC ON SPEC.SAMP_ID = SAMP.SAMP_ID INNER JOIN TXG ON TXG.SPEC_ID = SPEC.SPEC_ID WHERE LAB_PROGRAM_ID = 1”

This query returns the number of TXG_ID values from the TXG table where LAB_PROGRAM_ID = 1. To obtain this value, connections among tables must be performed using the foreign key structure established in the database schema. This is accomplished using INNER JOIN statements, which will join tables together where they share a common key.

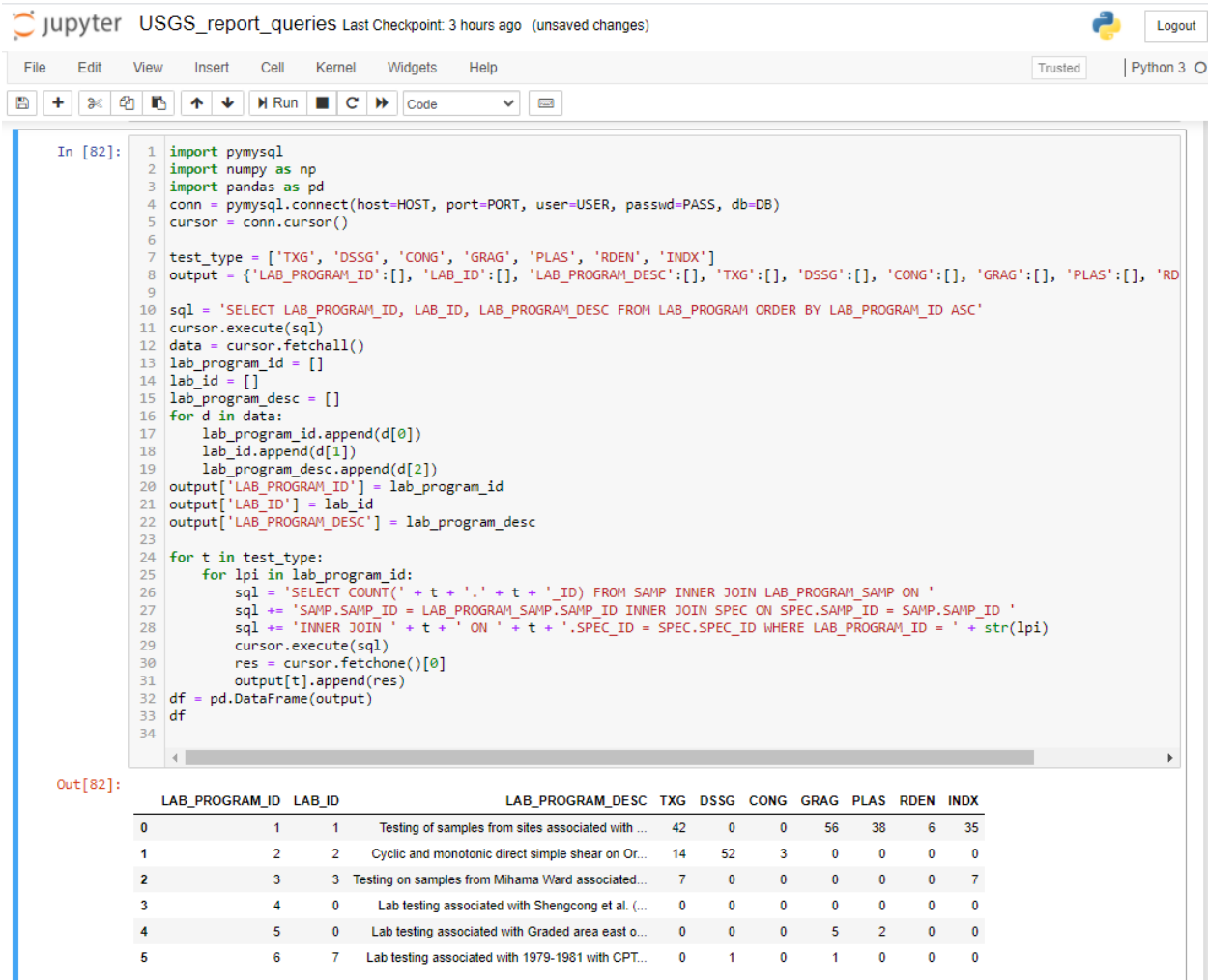


Figure 3.3 Example query of the number of tests of the various types stored in the NGL database.

A laboratory test viewer has been developed using Jupyter notebooks to query the laboratory component of the database and plot simple shear tests, triaxial tests, and consolidation that are stored within the database. Fig. 3.4 illustrates the lab viewer interface. The first code cell in Fig. 3.4 creates an object called “lv” that is created by instantiating the “lab_viewer” class contained within the “lab_viewer” package that is defined by a separate Python file that must be in the same folder as the Jupyter notebook. Once the object is created, a dropdown menu appears in which users can select the Lab Program they wish to view. In Fig. 3.4, the PDX-TS4 (Site E) site has been selected. Once a lab program is selected, users may then select a Sample from the dropdown menu. After selecting a Lab Program and Sample, metadata about the Laboratory, Lab Program, Sample, Specimen, and Stage then appear. By default, the first specimen associated with a sample, and the first load stage associated with a specimen are selected, though users can modify those selections using subsequent dropdown menus described shortly.

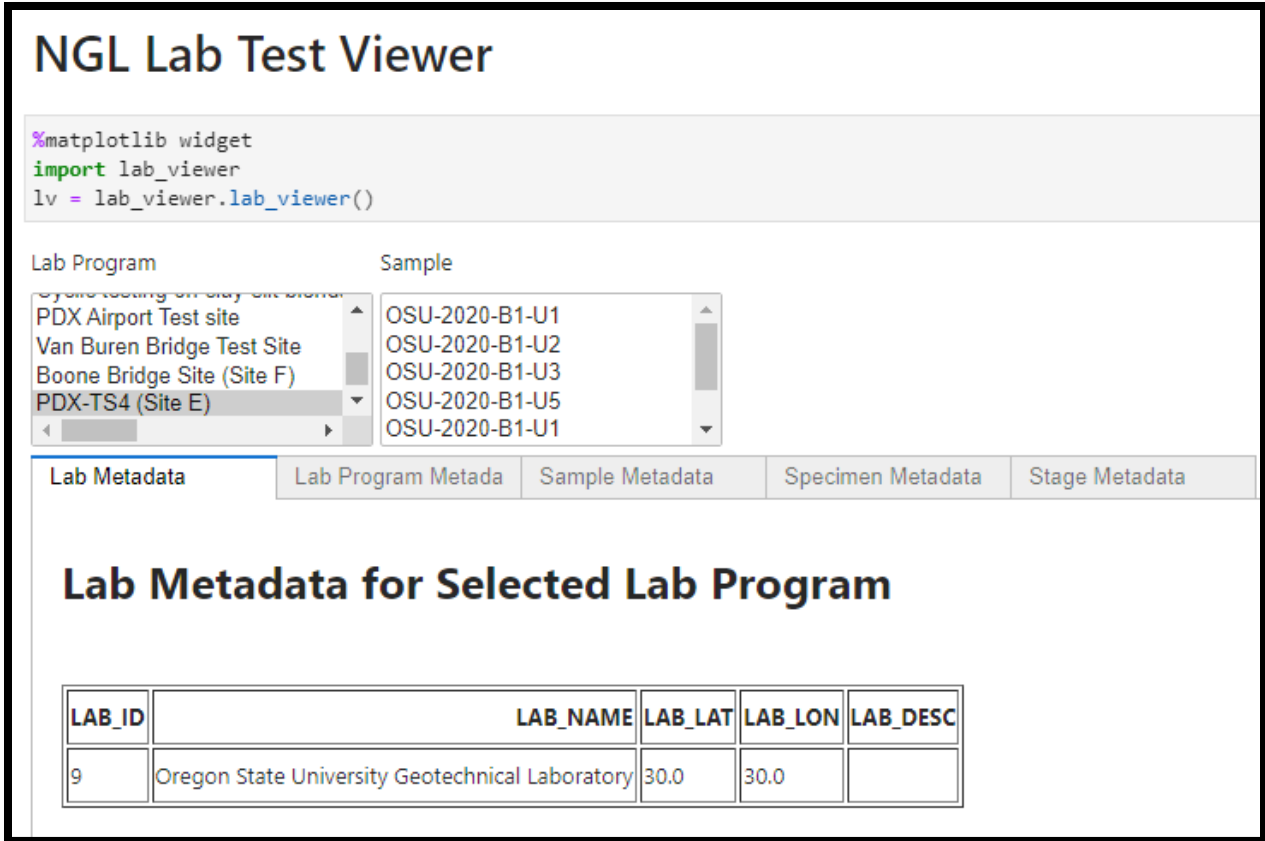


Figure 3.4 NGL laboratory test viewer GUI for selecting Lab Program and Sample.

After selecting a Lab Program and Sample in the dropdown menus in Fig. 3.4, tabbed display appears with different tabs corresponding to different tests available for the selected sample, as illustrated in Fig. 3.5. In this case, the selected sample has direct simple shear and consolidation tests. Users can then select a specimen and loading stage and relevant data are plotted. In Fig. 3.5, direct simple shear data are plotted for Specimen E-1-10, Stage 2. In this case, stress-strain data are plotted using a linear x-axis scale, and the stresses are not normalized by the initial consolidation stress. Users may opt to alter these selections to view time-series data on log or sqrt(time) scales, and also perhaps to normalize stress quantities by the consolidation stress. Additionally, Fig. 3.6 illustrates constant-rate-of-strain consolidation test data for the same sample. Although not shown in Figs. 3.5 and 3.6, users may save any set of plots as an image (e.g., .png, .tif, or .jpg file formats) by entering the filename and desired resolution, and pushing a “Save Figure” button.

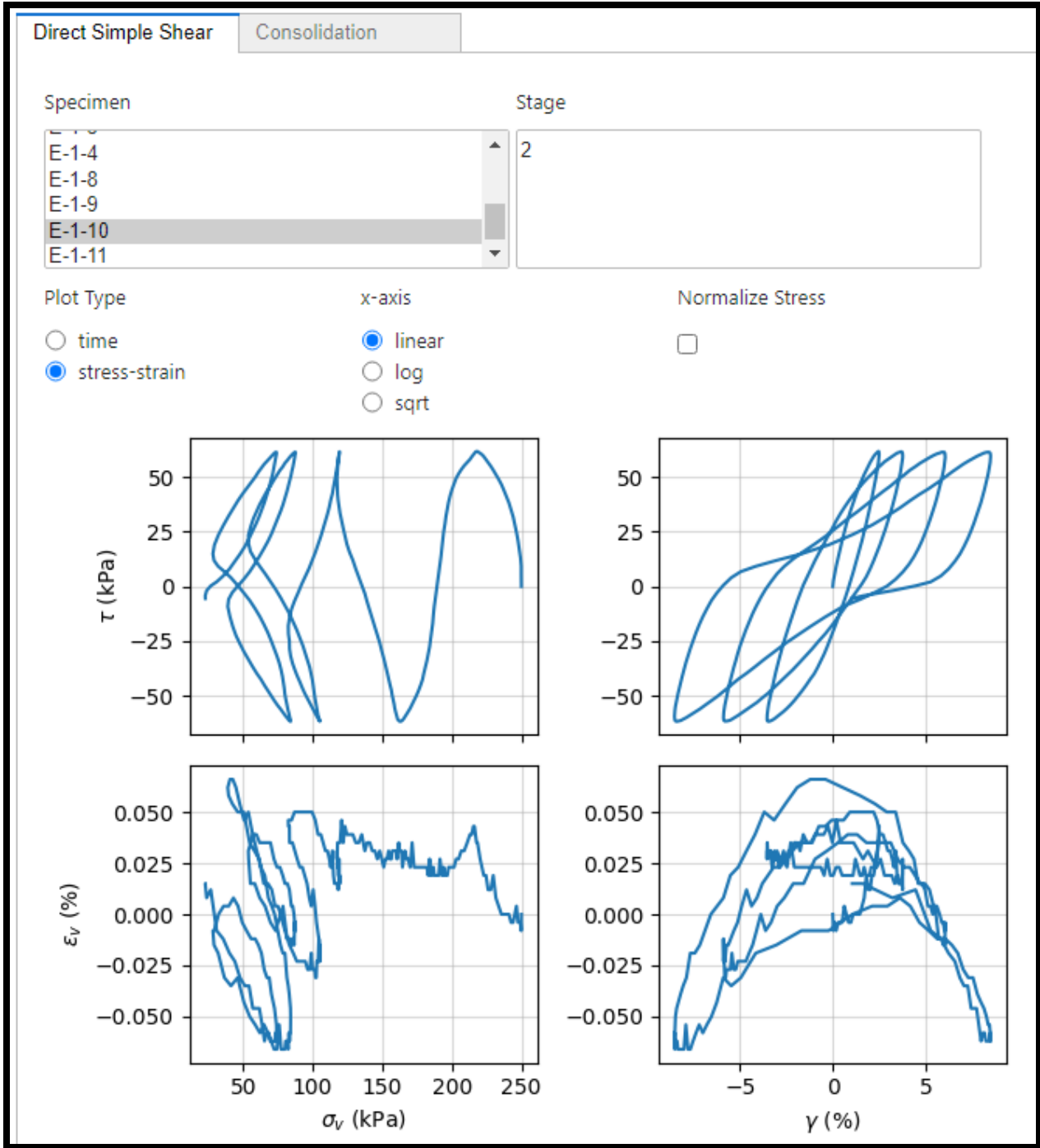


Figure 3.5 Direct simple shear test viewer example.

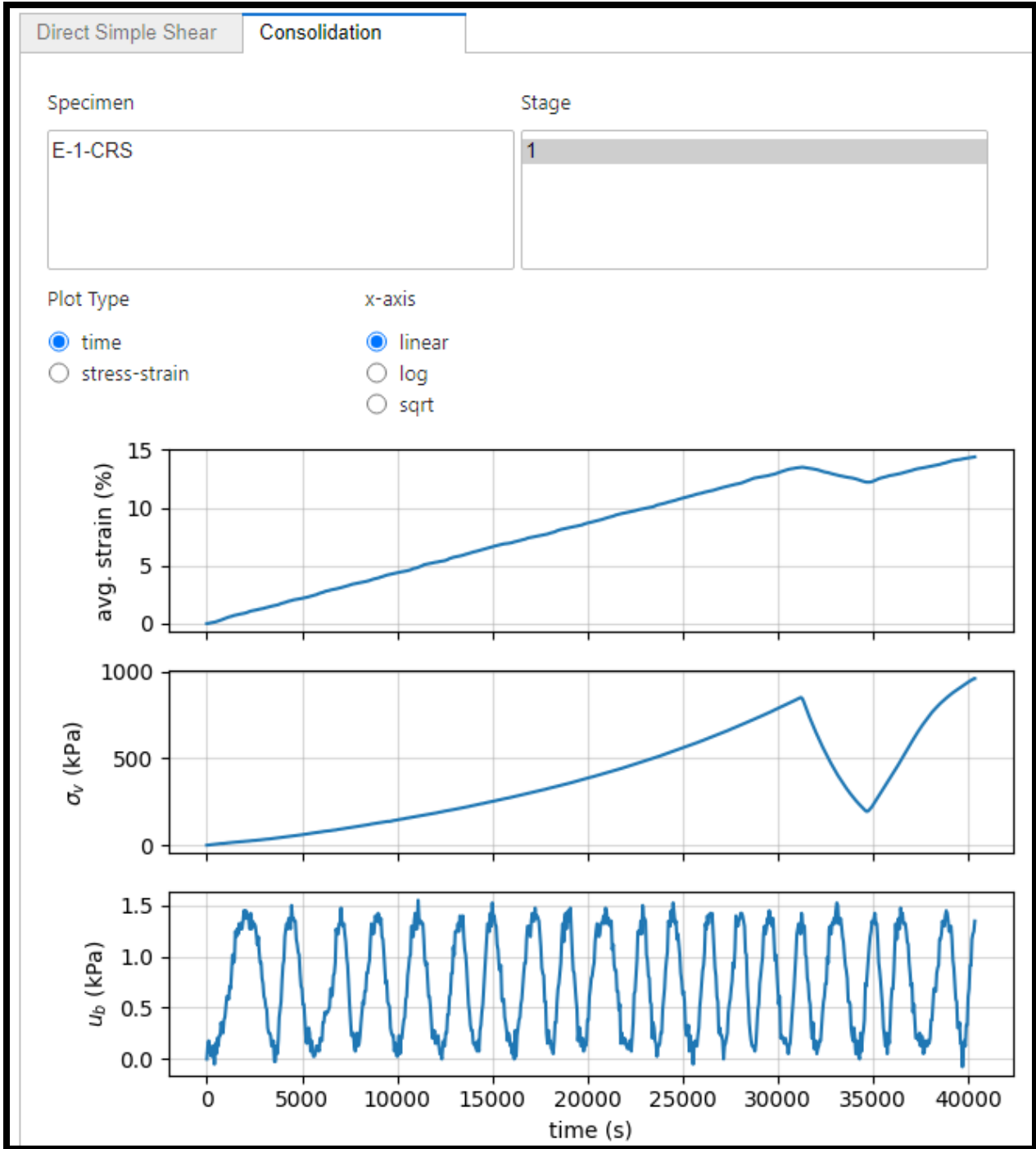


Figure 3.6 Consolidation test viewer example.

If users wish to perform more processing on the raw data quantities, or plot them in a manner not afforded by the lab viewer tool, the data associated with the selected Lab Program, Sample, Specimen, and Load Stage are accessible through the lab_viewer object. Accessible fields for direct simple shear tests include *dssg_time* (time array in seconds), *dssg_tau* (shear stress array in

kPa), *dssg_sigv* (vertical stress array in kPa), *dssg_yhv* (shear strain array in %), *dssg_epsv* (vertical strain array in %). Accessible fields for triaxial tests include *txg_time* (time array in seconds), *txg_Sd* (deviator stress in kPa), *txg_sigcp* (cell pressure in kPa), *txg_peff* (mean effective stress in kPa), *txg_ea* (axial strain in percent), *txg_ev* (volumetric strain in percent). Accessible fields for consolidation tests include *cong_time* (time array in seconds), *cong_epsv* (average vertical strain in percent), *cong_sigv* (vertical total stress in kPa), *cong_pp* (pore pressure at bottom of specimen in kPa, optional).

4 SUMMARY AND CONCLUSIONS

This report provides a study of patterns of liquefaction and non-liquefaction observed at Mihama Ward during the 2011 Tohoku earthquake. Our hypothesis at the beginning of the project was that susceptibility might explain the observed patterns of behavior, with sand-like soils exhibiting liquefaction and clay-like soils not exhibiting manifestation. However, we found this hypothesis to be only partially true. Locations where manifestations were observed did indeed correspond to sand-like soils that are susceptible to liquefaction. Furthermore, locations with high plasticity soils did not manifest liquefaction. However, we also encountered soils that did not exhibit surface manifestation, but were found to be non-plastic and therefore susceptible to liquefaction. The lack of manifestation at these locations therefore cannot be attributed to plasticity characteristics, as we had initially hypothesized.

Having ruled out our initial hypothesis, we turned our attention to evaluating each profile using the Boulanger and Idriss (2016) CPT liquefaction model. We found that the model correctly predicted manifestation at sites where manifestation was observed (i.e., true positives). However, we also found that the model incorrectly predicted manifestation at sites where none was observed (i.e., false positives). The model did not produce any negative predictions, though one point is very close to the 50% probability threshold. We postulate that reasons for the false positives include the following: 1. Interbedded soils may suppress manifestation, even when liquefaction triggering occurs, because layers of liquefied soil are thin and separated from each other by layers of non-liquefied soil, 2. Liquefied layers may be too deep to produce measurable surface manifestations (i.e., sand boils, ground cracks, etc.), and/or 3. A thick/strong capping layer may suppress manifestation of underlying liquefiable layers.

The Next Generation Liquefaction relational database was expanded to include a laboratory component containing direct simple shear, triaxial, and consolidation test data. Data from four (4) different laboratories and nine (9) different laboratory test programs are currently in the database. A lab test viewer was created to enable users to visualize the data, and further interact with it in their own custom workflows.

REFERENCES

- Beyzaei, C. Z. 2017. "Fine-Grained Soil Liquefaction Effects in Christchurch, New Zealand." UC Berkeley.
- Bodenmann, L., J. W. Baker, and B. Stojadinović. 2023. "Accounting for path and site effects in spatial ground-motion correlation models using Bayesian inference." *Nat. Hazards Earth Syst. Sci.*, 23 (7): 2387–2402. Copernicus GmbH. <https://doi.org/10.5194/nhess-23-2387-2023>.
- Boulanger, R.W., and I.M. Idriss 2004. "Evaluating the Potential for Liquefaction or Cyclic Failure of Silts and Clays." UCD/CGM-04/01, Center for Geotechnical Modeling, Department of Civil & Environmental Engineering, University of California, Davis, 131 p.
- Boulanger, R. W., and I. M. Idriss. 2007. "Evaluation of Cyclic Softening in Silts and Clays." *J. Geotech. Geoenvironmental Eng.*, 133 (6): 641–652. [https://doi.org/10.1061/\(ASCE\)1090-0241\(2007\)133:6\(641\)](https://doi.org/10.1061/(ASCE)1090-0241(2007)133:6(641)).
- Boulanger, R. W., and I. M. Idriss. 2016. "CPT-Based Liquefaction Triggering Procedure." *J. Geotech. Geoenvironmental Eng.*, 142 (2): 04015065. [https://doi.org/10.1061/\(ASCE\)GT.1943-5606.0001388](https://doi.org/10.1061/(ASCE)GT.1943-5606.0001388).
- Brandenberg, S. J., and I. M. Idriss. 2022. "An overview of the great Alaska earthquake of 1964."
- Bray, J. D., and R. B. Sancio. 2006. "Assessment of the Liquefaction Susceptibility of Fine-Grained Soils." *J. Geotech. Geoenvironmental Eng.*, 132 (9): 1165–1177. [https://doi.org/10.1061/\(ASCE\)1090-0241\(2006\)132:9\(1165\)](https://doi.org/10.1061/(ASCE)1090-0241(2006)132:9(1165)).
- Bray, J. D., R. B. Sancio, T. Durgunoglu, A. Onalp, T. L. Youd, J. P. Stewart, R. B. Seed, O. K. Cetin, E. Bol, M. B. Baturay, C. Christensen, and T. Karadayilar. 2004. "Subsurface Characterization at Ground Failure Sites in Adapazari, Turkey." *J. Geotech. Geoenvironmental Eng.*, 130 (7): 673–685. [https://doi.org/10.1061/\(ASCE\)1090-0241\(2004\)130:7\(673\)](https://doi.org/10.1061/(ASCE)1090-0241(2004)130:7(673)).
- Chu, D. B., J. P. Stewart, R. W. Boulanger, and P. S. Lin. 2008. "Cyclic Softening of Low-Plasticity Clay and Its Effect on Seismic Foundation Performance." *J. Geotech. Geoenvironmental Eng.*, 134 (11): 1595–1608. [https://doi.org/10.1061/\(ASCE\)1090-0241\(2008\)134:11\(1595\)](https://doi.org/10.1061/(ASCE)1090-0241(2008)134:11(1595)).
- Cubrinovski, M., A. Rhodes, N. Ntritsos, and S. Van Ballegooy. 2019. "System response of liquefiable deposits." *Soil Dyn. Earthq. Eng.*, 124: 212–229. <https://doi.org/10.1016/j.soildyn.2018.05.013>.
- Eslami, M. 2017. *Experimental mapping of elastoplastic surfaces for sand and cyclic failure of low-plasticity fine-grained soils*. University of California, Los Angeles.
- Hansen, W. R. 1965. *Effects of the earthquake of March 27, 1964, at Anchorage, Alaska*. Prof. Pap. U.S. Government Printing Office.
- Hudson, K. S., P. Zimmaro, K. Ulmer, B. Carlton, A. Stuedlein, A. Jana, A. Dadashiserej, S. J. Brandenberg, J. Stamatakos, S. L. Kramer, and J. P. Stewart. 2022. "Laboratory Component of Next-Generation Liquefaction Project Database." *Proc. 4th Int. Conf. Perform. Based Des. Earthq. Geotech. Eng. Beijing 2022*, Geotechnical, Geological and Earthquake Engineering, L. Wang, J.-M. Zhang, and R. Wang, eds., 1865–1874. Cham: Springer International Publishing.

- Idriss, I. M. 1985. "Evaluating seismic risk in engineering practice: XI International Conference on Soil Mechanics and Foundation Engineering, San Francisco, 12-16 AUGUST 1985." *Publ. Balkema AA*.
- Kwak, D. Y., D. Park, and H.-K. Kim. 2011. "Probabilistic seismic site coefficients of Korea." *14th Asian Reg. Conf. Soil Mech. Geotech. Eng.*
- Nakai, S., and T. Sekiguchi. 2013. "Analysis of liquefaction damage in Mihama-ku of Chiba city due to 2011 Tohoku earthquake." *BUTSURI-TANSAGEophysical Explor.*, 66 (1): 37–43. <https://doi.org/10.3124/segj.66.37>.
- Pretell, R., S. J. Brandenburg, and J. P. Stewart. 2024. "Consistent framework for PGA estimation at liquefaction case history sites: Application to the 1989 Loma Prieta Earthquake." *GeoCongress 2024*.
- Rathje, E. M., C. Dawson, J. E. Padgett, J.-P. Pinelli, D. Stanzione, A. Adair, P. Arduino, S. J. Brandenburg, T. Cockerill, C. Dey, M. Esteva, F. L. Haan, M. Hanlon, A. Kareem, L. Lowes, S. Mock, and G. Mosqueda. 2017. "DesignSafe: New Cyberinfrastructure for Natural Hazards Engineering." *Nat. Hazards Rev.*, 18 (3): 06017001. American Society of Civil Engineers. [https://doi.org/10.1061/\(ASCE\)NH.1527-6996.0000246](https://doi.org/10.1061/(ASCE)NH.1527-6996.0000246).
- Sancio, R. B. 2003. *Ground failure and building performance in Adapazari, Turkey*.
- Seed, H. B., and I. M. Idriss. 1982. *Ground Motions and Soil Liquefaction During Earthquakes*. Earthquake Engineering Research Institute.
- Sekiguchi, T., and S. Nakai. 2012. "Effects of local site conditions on liquefaction damage in Mihama ward of Chiba City." *Proc. Int. Symp. Eng. Lessons Learn. 2011 Gt. East Jpn. Earthq.*, 865–870.
- Tokyo Soils. 2016. *Report of Soil Testing Results for Mihama Ward*. Tokyo Soils Research Company. Japan.
- Tsukamoto, Y., S. Kawabe, J. Matsumoto, and S. Hagiwara. 2014. "Cyclic resistance of two unsaturated silty sands against soil liquefaction." *Soils Found.*, 54 (6): 1094–1103. <https://doi.org/10.1016/j.sandf.2014.11.005>.
- Ulmer, K., P. Zimmaro, S. J. Brandenburg, J. P. Stewart, K. S. Hudson, A. W. Stuedlein, A. Jana, A. Dadashiserej, S. L. Kramer, H. Dacayanan, D. Y. Kwak, J. Stamatakos, J. Mukherjee, U. Salman, S. Ybarra, and T. Weaver. 2023. "Next-generation liquefaction database, version 2. next-generation liquefaction consortium. DOI: 10.21222/C23P70. <https://doi.org/10.21222/C23P70>"
- Wang, W. 1979. *Some Findings in Soil Liquefaction*. Earthquake Engineering Department, Water Conservancy and Hydroelectric Power Scientific Research Institute.

APPENDIX A

TRIAXIAL TEST DATA

All triaxial test data performed at Tokyo Soil, Inc. for specimens trimmed from samples collected at Mihama Ward are plotted below.

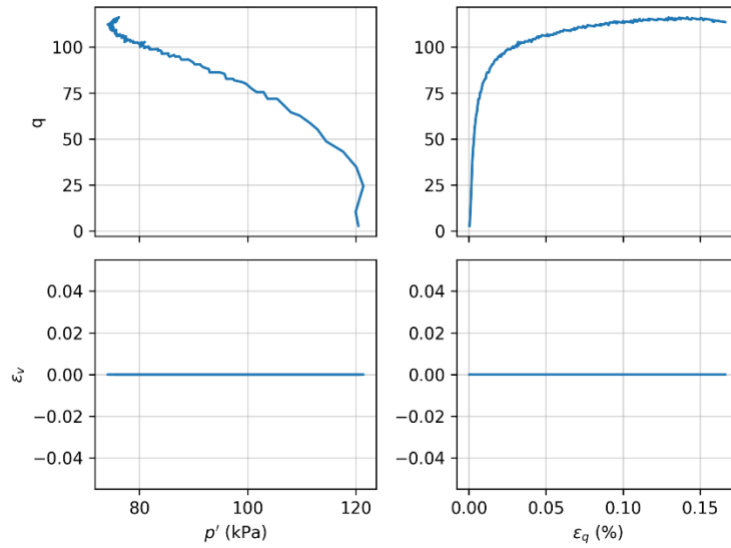


Figure A.1. Triaxial test on B6, sample S-1 for stage 1.

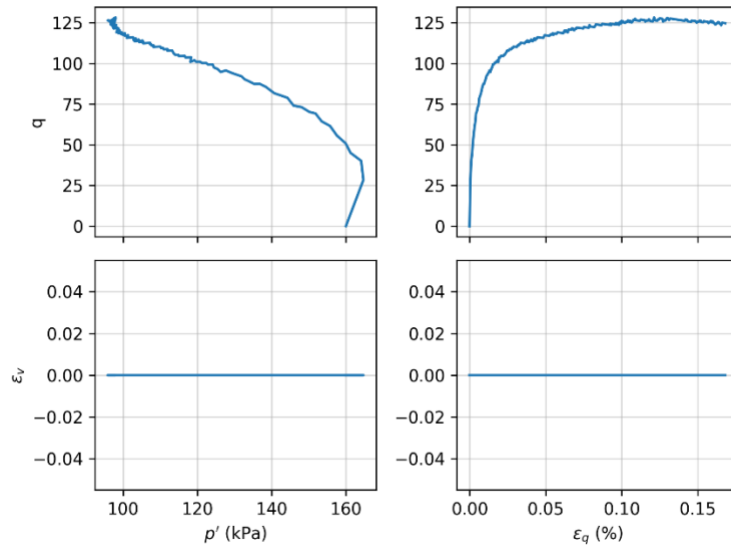


Figure A.2. Triaxial test on B6, sample S-1 for stage 2.

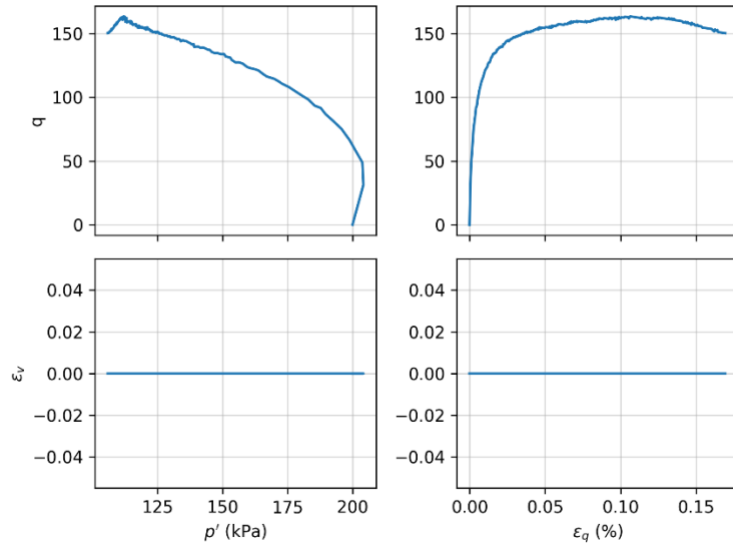


Figure A.3. Triaxial test on B6, sample S-1 for stage 3.

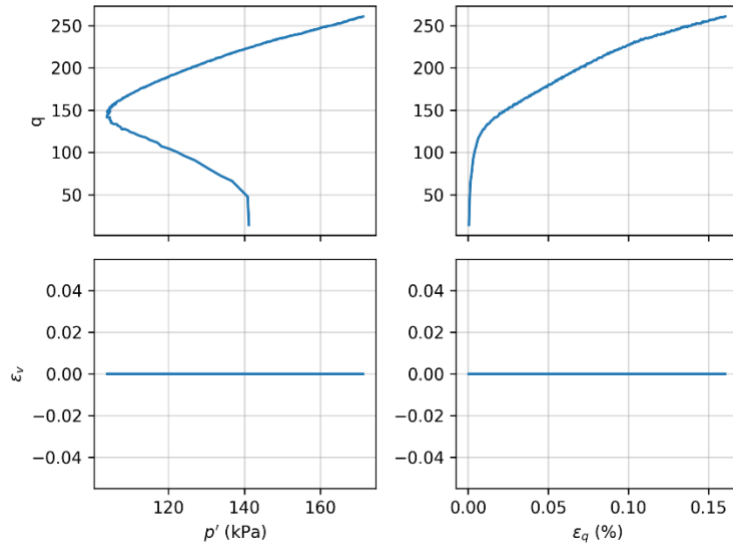


Figure A.4. Triaxial test on B1, sample S-2, for stage 1.

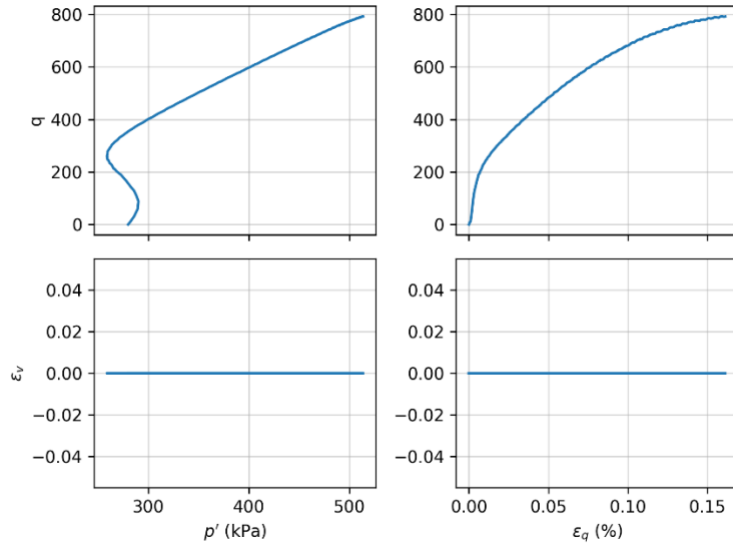


Figure A.5. Triaxial test on B1, sample S-2, for stage 2.

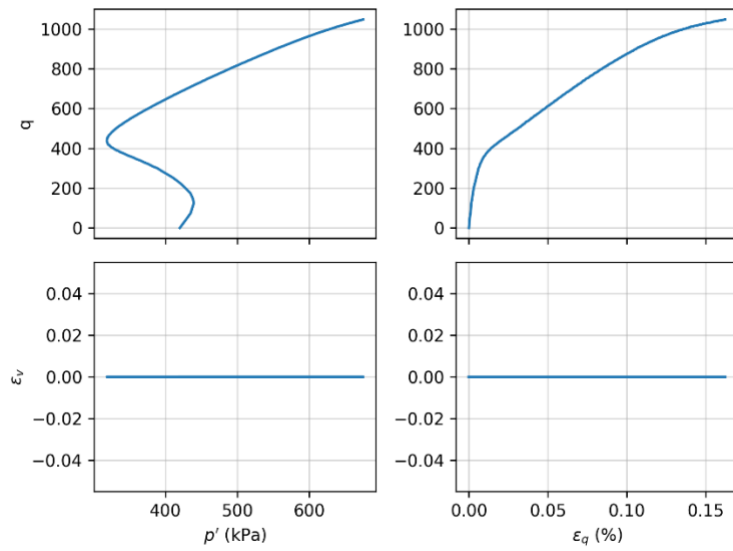


Figure A.6. Triaxial test on B1, sample S-2, for stage 3.

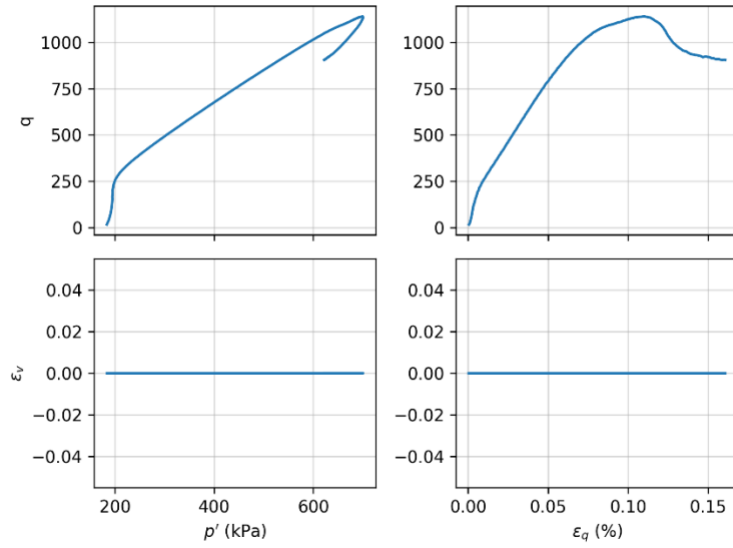


Figure A.7. Triaxial test on B1, sample S-3, for stage 1.

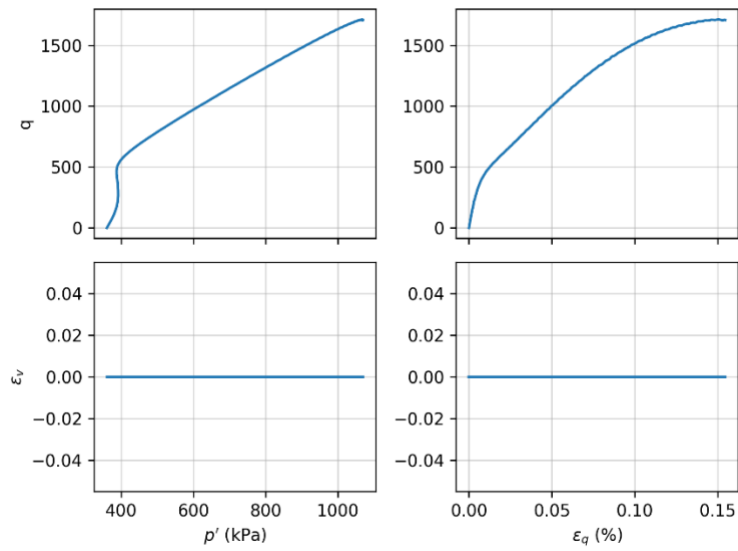


Figure A.8. Triaxial test on B1, sample S-3, for stage 2.

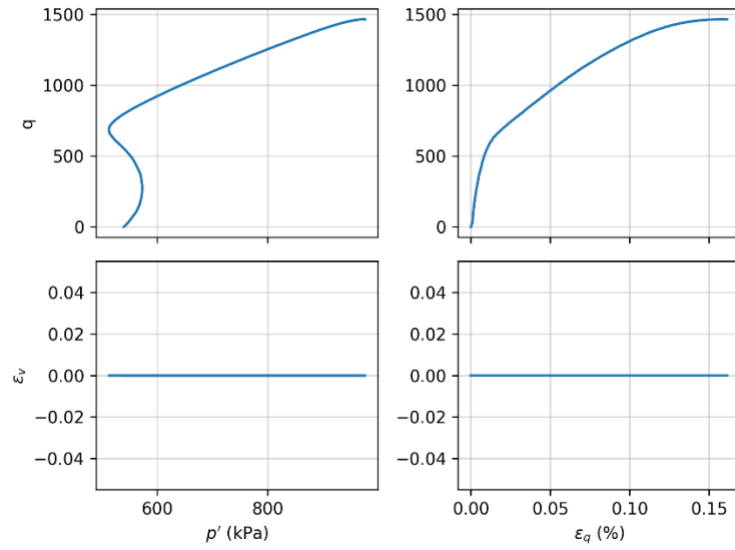


Figure A.9. Triaxial test on B1, sample S-3, for stage 3.

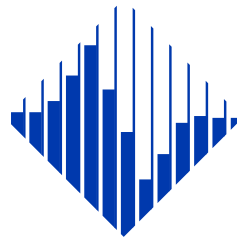
Disclaimer

The opinions, findings, and conclusions or recommendations expressed in this publication are those of the author(s) and do not necessarily reflect the views of the study sponsor(s), the Pacific Earthquake Engineering Research Center, or the Regents of the University of California.

The Pacific Earthquake Engineering Research Center (PEER) is a multi-institutional research and education center with headquarters at the University of California, Berkeley. Investigators from over 20 universities, several consulting companies, and researchers at various state and federal government agencies contribute to research programs focused on performance-based earthquake engineering.

These research programs aim to identify and reduce the risks from major earthquakes to life safety and to the economy by including research in a wide variety of disciplines including structural and geotechnical engineering, geology/seismology, lifelines, transportation, architecture, economics, risk management, and public policy.

PEER is supported by federal, state, local, and regional agencies, together with industry partners.



PEER Core Institutions

University of California, Berkeley (Lead Institution)
California Institute of Technology
Oregon State University
Stanford University
University of California, Davis
University of California, Irvine
University of California, Los Angeles
University of California, San Diego
University of Nevada, Reno
University of Southern California
University of Washington

Pacific Earthquake Engineering Research Center
University of California, Berkeley
325 Davis Hall, Mail Code 1792
Berkeley, CA 94720-1792
Tel: 510-642-3437
Email: peer_center@berkeley.edu

ISSN 2770-8314
<https://doi.org/10.55461/AMNH7013>